Journal of Modern Optics
Vol. 52, No. 12, 15 August 2005, 1695–1728

Taylor & Francis
Taylor & Francis Group

Aberration retrieval from the intensity point-spread function in the focal region using the extended Nijboer–Zernike approach

C. VAN DER AVOORT*†, J. J. M. BRAAT†,
P. DIRKSEN‡ and A. J. E. M. JANSSEN‡

†Optics Research Group, Faculty of Applied Sciences,
Delft University of Technology, 2628 CJ Delft, The Netherlands
‡Philips Research Laboratories, 5656 AA Eindhoven, The Netherlands

(*Received 13 January 2005*)

A recently found extension of the Nijboer–Zernike approach to optical aberrations allows analytic computation of the intensity point-spread function in the focal region of an optical system. Here, the exit pupil function is expanded as a Zernike series $\sum_{n,m} \beta_n^m Z_n^m$, with β_n^m a complex coefficient of the single aberration Z_n^m, and the contribution of each of the terms of this series to the complex-amplitude point-spread function U in the focal region has an analytic form. This representation of U, and hence of the intensity point-spread function $I = |U|^2$, is highly efficient since normally a pupil function is already accurately described by a few β's.

In this paper, the inverse problem of retrieving the β's from a given intensity I in the focal region is studied. A computation scheme for solving this nonlinear estimation problem, under the assumption of small-to-medium–large aberrations, is proposed. The key step is to linearize the theoretical intensity, comprising the β's as unknowns, by deleting second-order terms, and to optimize the match between the linearized, theoretical intensity and the given intensity in the focal region. The special case of a small pure-phase aberration pupil function is separately considered. For general pupil functions (also containing amplitude errors) or larger pure-phase aberrations, the linearization error(s) cannot be ignored. By adopting a predictor–corrector approach, the effect of linearization can be eliminated iteratively and this yields accurate or even perfect retrieval of aberrations well beyond the diffraction limit.

Although the method was developed for lithographic applications, with numerical apertures ≤ 0.60 and almost-ideal point sources, it has potential applications to more general light optics settings (microscopy, astronomy, ...). The application range of the method is, furthermore, extended in this paper to cover the medium–high numerical aperture range (≤ 0.80) and to the case that the lateral size of the illumination source is comparable to the diffraction unit.

The paper is explorative in nature and aims at illustrating the potential and key features of the methods, on the whole by showing results from simulations. Accordingly, little effort has been spent on addressing the many fundamental aspects of a mathematical, statistical and modelling nature; a list containing these fundamental issues is included at the end of the paper.

*Corresponding author. Email: c.vanderavoort@tnw.tudelft.nl

Journal of Modern Optics
ISSN 0950–0340 print/ISSN 1362–3044 online
http://www.tandf.co.uk/journals
DOI: 10.1080/09500340500072547

1. Introduction

1.1 *Motivation*

The present research effort is motivated by the ever increasing and changing needs in optical lithography for methods to characterize aberrated lenses. The application range of the method proposed in this paper is, however, by no means restricted to lithography; we envisage applications of it also in fields like (scanning) microscopy, astronomy, adaptive optics.

The increased interest in qualification methods for lithographic projection lenses can be explained from the circumstance that projection lens aberrations have an important contribution to line width variations and image misplacements [1, 2]. The impact of these aberrations increases with each new technology node due to the small dimensions of the optical systems compared to the exposure wavelength. To minimize this impact, modern lithographic lenses have a number of manipulators to tune specific aberrations such as focal plane deviation, astigmatism, coma and spherical aberrations. Although the lens manufacturer delivers a well optimized lens, the advanced user needs to balance lens aberrations for optimal performance on specific patterns. In addition, aberrations may vary with time due to lens aging and machine drift.

Although several user tests are available, such as an *in situ* interferometer or various resist-based methods [3–6], we have proposed in [7] a new approach. This approach is based on the observation of the intensity point-spread function in the focal region from which we can extract the significant Zernike coefficients in the Zernike series representation $\sum_{n,m} \beta_n^m Z_n^m(\rho, \vartheta)$ of the exit pupil function $P(\rho, \vartheta)$. This approach has several advantages. In interferometric methods, the complex amplitude U of the point-spread function is required while often only the intensity $I = |U|^2$ of the point-spread function is available. Furthermore, interferometry requires expensive coherent sources with appropriate wavelengths, and the skills to operate these sources are not readily available in a production environment. In contrast, our method is straightforward from an experimental point of view, the test pattern being as simple as possible: an isolated transparent hole in a dark field binary mask.

Our method can be categorized as a phase-retrieval method for which numerous approaches are available in the literature [8–21]. Our approach is new in the sense that we use the highly efficient representation of pupil functions by means of their Zernike coefficients. These coefficients are estimated by using a matching procedure in the focal region between the (linearized) theoretical intensity point-spread function (comprising the coefficients as the quantities to be estimated) and the measured intensity point-spread function. The reason why an approach such as the present one has not been tried before is probably the fact that until recently no analytical scheme was available for the evaluation of the contributions of the single aberration terms $Z_n^m(\rho, \vartheta)$ to the amplitude or intensity of the point-spread function in the focal region (and not just at best focus). This obstacle has been removed in [22], and this has led us to propose the retrieval method as appears in [7] which we will discuss now in more detail.

1.2 *Zernike representation and retrieval for pure-phase aberrations*

Although our retrieval method is capable of reconstructing general pupil functions, comprising both amplitude and phase defects, we first treat in this subsection the case where the optical system introduces a wavefront aberration only. This is also historically the path along which the Zernike polynomials have been applied in optics. They were meant to describe, in a stable and orthogonal way, aberrations of various types and the order of a designed or manufactured optical system. The more versatile description using the β-coefficients for a pupil function affecting amplitude and phase will then follow as a generalization of the phase-only analysis in this subsection.

Assuming a pure-phase aberration we write the pupil function P in normalized coordinates as

$$P(\rho, \vartheta) = \exp[\mathrm{i}\Phi(\rho, \vartheta)], \quad 0 \le \rho \le 1, \quad 0 \le \vartheta \le 2\pi, \tag{1}$$

with Φ the real-valued aberration phase. This Φ is thought to be expanded as a Zernike series

$$\Phi = \sum_{n,m} \alpha_n^m Z_n^m, \tag{2}$$

with real α_n^m and Zernike functions Z_n^m given as

$$Z_n^m(\rho, \vartheta) = R_n^m(\rho) \begin{cases} \cos m\vartheta, \\ \sin m\vartheta, \end{cases} \quad 0 \le \rho \le 1, \quad 0 \le \vartheta \le 2\pi, \tag{3}$$

with R_n^m the Zernike polynomials in standard convention, see [23], section 9.2 and Appendix VII. The summation in (2) is over all integer $n, m \ge 0$ with $n - m \ge 0$ and even. We shall make the usual symmetry assumption on Φ, $\Phi(\rho, -\vartheta) = \Phi(\rho, \vartheta)$, so that only the cosine option on the right-hand side of (3) needs to be considered. (The general case can be treated by working with two sets of α-coefficients, one for the cosine and one for the sine option in (3).) The α's in the expansion in (2) carry physical significance: α_2^0 represents defocus, α_1^1 represents tilt, α_2^2 represents astigmatism, α_4^0 represents spherical aberration, α_3^1 represents coma, etc. (also see [23], section 9.2 for this matter). The complex amplitude at normalized defocus parameter f of the point-spread function is denoted by U and follows from Fourier optics as

$$\begin{aligned} U(x, y; f) &\equiv U(r, \varphi; f) \\ &= \frac{1}{\pi} \int_{\nu^2+\mu^2 \le 1} \int \exp[\mathrm{i}f(\nu^2 + \mu^2) + \mathrm{i}\Phi(\nu, \mu)] \exp[2\pi\mathrm{i}\nu x + 2\pi\mathrm{i}\mu y] \, \mathrm{d}\nu \, \mathrm{d}\mu \\ &= \frac{1}{\pi} \int_0^1 \int_0^{2\pi} \exp[\mathrm{i}f\rho^2] \exp[\mathrm{i}\Phi(\rho, \vartheta)] \exp[2\pi\mathrm{i}\rho r \cos(\vartheta - \varphi)] \rho \, \mathrm{d}\rho \, \mathrm{d}\vartheta. \end{aligned} \tag{4}$$

With some abuse of notation, we have used here Cartesian coordinates ν, μ and polar coordinates in the exit pupil $[(\nu, \mu) = (\rho \cos\vartheta, \rho \sin\vartheta)]$, and Cartesian coordinates x, y and polar coordinates in the focal planes $[(x, y) = (r \cos\varphi, r \sin\varphi)]$. The relationship between normalized image coordinates (x, y) and defocus parameter f on one hand and the image coordinates (X, Y, Z) in the lateral and axial direction is given by

$$x = X \frac{2\pi \mathrm{NA}}{\lambda}, \quad y = Y \frac{2\pi \mathrm{NA}}{\lambda}, \quad f = \frac{\pi \mathrm{NA}^2}{\lambda} Z, \tag{5}$$

with NA the numerical aperture of the lens and λ the wavelength of the used light. In all this, we assume NA sufficiently small, say $\mathrm{NA} \leq 0.60$, so that certain approximations are permitted; in particular, the third formula in (5) follows from linearizing the true focal quantity $2\pi Z\lambda^{-1}(1-(1-\mathrm{NA}^2)^{1/2})$ as $\pi \mathrm{NA}^2 Z\lambda^{-1}$.

Under the assumption that Φ is sufficiently small, we may linearize the $\exp[\mathrm{i}\Phi]$, and inserting (2)–(3), we get

$$\exp[\mathrm{i}\Phi(\rho,\vartheta)] \approx 1 + \mathrm{i}\Phi(\rho,\vartheta) = 1 + \mathrm{i}\sum_{n,m} \alpha_n^m R_n^m(\rho)\cos m\vartheta. \tag{6}$$

Using that for integer m

$$\int_0^{2\pi} \exp[\mathrm{i}z\cos(\vartheta-\varphi)]\exp(\mathrm{i}m\vartheta)\,\mathrm{d}\vartheta = 2\pi\mathrm{i}^m \exp(\mathrm{i}m\varphi)J_m(z), \tag{7}$$

with J_m the Bessel function of the first kind and of order m, we can carry out the integration over ϑ in the integral in (4) term-by-term by inserting the right-hand side expression in (6). There results

$$U(r,\varphi;f) \approx 2V_0^0(r,f) + 2\mathrm{i}\sum_{n,m} \mathrm{i}^m \alpha_n^m V_n^m(r,f)\cos m\varphi, \tag{8}$$

where

$$V_n^m(r,f) = \int_0^1 \rho \exp(\mathrm{i}f\rho^2) R_n^m(\rho) J_m(2\pi r\rho)\,\mathrm{d}\rho. \tag{9}$$

In [22] and [24] we have presented series representations for the integrals in (9). The representation in [22] is a generalization of Lommel's representation of the aberration-free point-spread function, see [23], subsection 8.8.1, and reads

$$V_n^m(r,f) = \exp(\mathrm{i}f)\sum_{l=0}^{\infty}\left(\frac{-\mathrm{i}f}{\pi r}\right)^l \sum_{j=0}^{p} u_{lj}\frac{J_{m+l+2j+1}(2\pi r)}{2\pi r}, \tag{10}$$

where

$$u_{lj} = (-1)^p \frac{m+l+2j+1}{q+l+j+1}\binom{m+j+l}{l}\binom{j+l}{l}\binom{l}{p-j}\Big/\binom{q+l+j}{l}, \tag{11}$$

for $l = 0, 1, \ldots$ and $j = 0, 1, \ldots, p$, and where we have set $p = 1/2(n-m)$, $q = 1/2(n+m)$. This representation can be used for values of $|f|$ as large as 10π, where as a rule of thumb some $3|f|$ terms in the infinite series over l at the right-hand side of (10) are required, see [25], Appendix B. The series representation of V_n^m given in [24] is somewhat more complicated, involving both spherical Bessel functions and Bessel functions of the first kind and integer order, but has the advantage that it can be used for any value of f (and r). For our present purposes $|f|$ does not exceed 4π, and so the representation in (10)–(11) is sufficient.

The term $2V_0^0$ at the right-hand side of (8) corresponds to the aberration-free pupil function $P \equiv 1$. For relatively small aberrations, this term dominates the totality of all other terms. Accordingly, we write the intensity point-spread function $I = |U|^2$ as

$$I(r,\varphi;f) = 4|V_0^0(r,f)|^2 - 8\sum_{n,m}\alpha_n^m \,\mathrm{Im}\,[\mathrm{i}^m V_n^m(r,f)V_0^{0*}(r,f)]\,\cos m\varphi + C(r,\varphi;f), \tag{12}$$

where

$$C(r,\varphi;f) = 4\sum_{n_1,m_1;n_2,m_2}\alpha_{n_1}^{m_1}\alpha_{n_2}^{m_2}\,\mathrm{Re}[\mathrm{i}^{m_1-m_2}V_{n_1}^{m_1}(r,f)V_{n_2}^{m_2*}(r,f)]\cos m_1\varphi\cos m_2\varphi \tag{13}$$

comprises all second-order cross-terms.

Formula (12) shows how one can compute the intensities in the focal planes from the Zernike coefficients α of the pure-phase aberration Φ (assuming that $\exp[\mathrm{i}\Phi]$ may be linearized). The inverse problem, in which the α's are computed from the intensity I is, in principle, awkward due to the C term at the right-hand side of (12) involving the α's quadratically. In section 3 we present a strategy for handling equation (12) in which the C term disappears altogether from the formulas, leaving us with a set of linear systems in α (decoupled per azimuthal order m) which can easily be solved. Thus, within this procedure, it is permitted to delete C.

The procedure detailed in section 3 to compute α's from intensities I forms the basis for the aberration retrieval [pure phase] algorithm in this paper. Thus we assume to have available recorded intensity functions I_{meas}. The subscript 'meas' serves here to distinguish from the 'theoretical' intensity I in equation (12); we do not have a particular measurement procedure in mind at this point. Applying the procedure of section 3, with I at the left-hand side of (12) replaced by I_{meas}, we find α's that we consider to describe the pupil function that gave rise to the recorded I_{meas}. We are intentionally somewhat vague in this formulation since it is not so that the α's thus obtained minimize a mean-squared error between I_{meas} and the right-hand side of (12) including the C term. Nevertheless, in the sequel we shall somewhat loosely use phrases like 'best match' approach for the procedure of obtaining α's as is done in section 3.

2. Overview

In section 3 we present the details of the aberration retrieval method as outlined in subsection 1.2. In particular, we shall be more precise about the matching procedure. It will turn out that choosing a symmetric f-range and sampling in the image planes consistent with the choice of polar coordinates (r,φ) has considerable advantages. For instance, the linear systems that we construct for estimating the α_n^m decouple per m. Secondly, the linearization step (6) comes with an error of third-and-higher order only. At the end of section 3 we shall present a number of simulations that demonstrate these and other points. Here, we also want to point out that the method has proved its validity in the practical context of characterizing lithographic projection lenses, see [7, 26–28]. As an illustration of this statement we have included figure 1 which shows results of a detuning experiment where we compare the nominal state of an imaging tool with a detuned state, in which the aberrations have been added intentionally, and for either state our retrieval method has been used to estimate the aberrations. See [27] for more details.

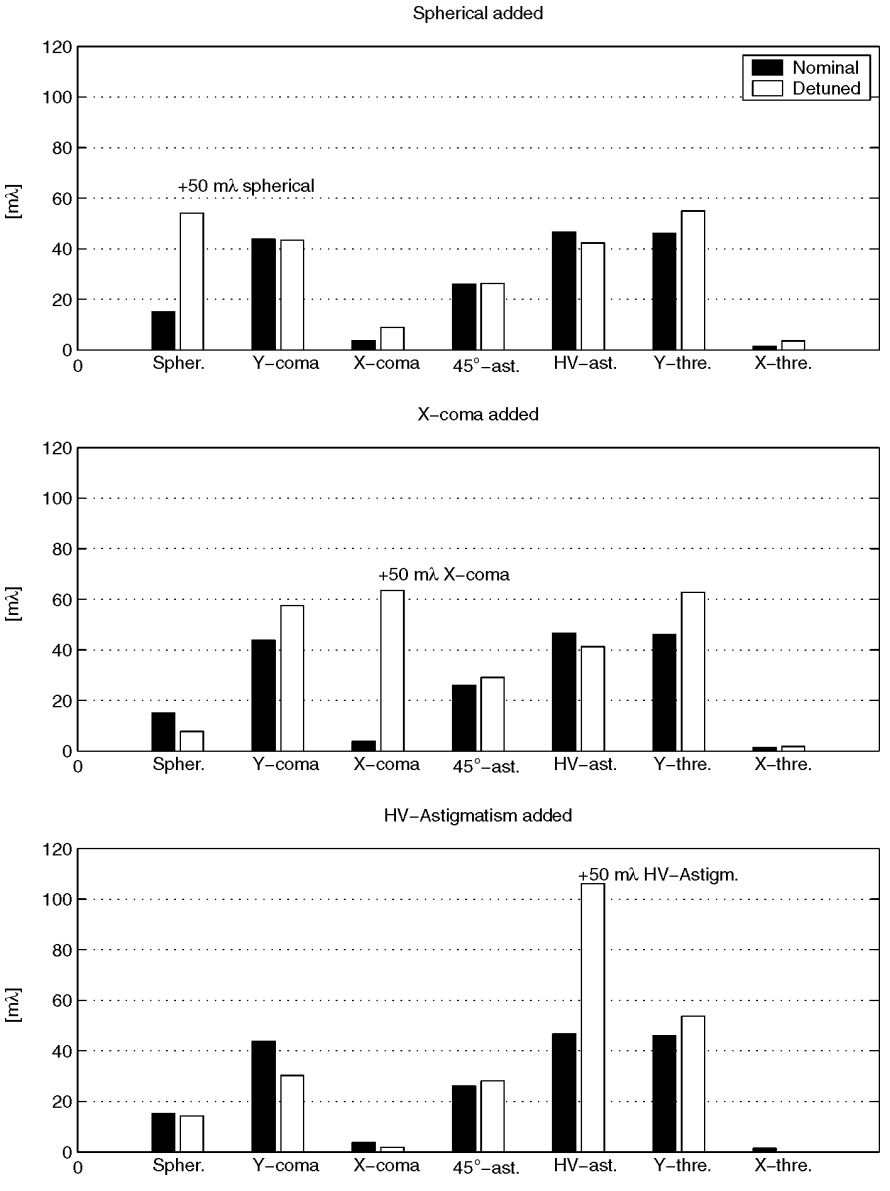

Figure 1. Detuning experiment in which aberrations are compared to nominal state imaging tool. Top: $+50m\lambda$ spherical aberration added, middle: $+50m\lambda$ X-coma added, bottom: $+50m\lambda$ HV-astigmatism added.

In section 4 we extend the method of section 3 (which was limited to retrieval of pure-phase aberrations) to the case of general pupil functions $P = A\exp[\mathrm{i}\Phi]$ with real aberration phase Φ and transmission non-uniformity $A \geq 0$. The pupil function P is now thought to be expanded as

$$P = A \exp[\mathrm{i}\Phi] = \sum_{n,m} \beta_n^m Z_n^m \tag{14}$$

with Z_n^m as before, see (3), and there results, in a similar manner as in (8), the representation

$$U = \sum_{n,m} \beta_n^m U_n^m; \quad U_n^m(r, \varphi; f) = 2i^m V_n^m(r, f) \cos m\varphi \tag{15}$$

of the point-spread function. The representation in (15) is exact since no linearization step was required. The β_n^m are general complex numbers. Thus when we expand $I = |U|^2$ as in (12), and concentrate on the cross-terms between V_n^m and V_0^0, we have to consider, in addition to the 'basis functions'

$$\mathrm{Im}[\mathrm{i}^m V_n^m(r, f) V_0^{0*}(r, f)] \cos m\varphi \tag{16}$$

that occur at the right-hand side of (12), the functions

$$\mathrm{Re}[\mathrm{i}^m V_n^m(r, f) V_0^{0*}(r, f)] \cos m\varphi. \tag{17}$$

The basic assumption is now that all β_n^m with $(n, m) \neq (0, 0)$ are relatively small compared to β_0^0. This β_0^0 can be taken to be positive since in our intensity-based method, the β_n^m can be retrieved only up to an overall phase factor.

The quantities to be estimated now are $\mathrm{Im}\,\beta_n^m$ and $\mathrm{Re}\,\beta_n^m$, and these occur as coefficients of the functions in (16) and (17), respectively, in the linearized intensity. As in section 3, these coefficients can be estimated by optimizing the match between (linearized) theoretical and recorded intensity. And, as in section 3, choosing a symmetric f-range and sampling the image planes (r, φ)-consistently has certain advantages.

In contrast with what we saw in the pure-phase retrieval method, the cross-terms involving two β_n^m's with $(m, n) \neq (0, 0)$ do not vanish altogether when the procedure of section 3 is applied. By adopting an iterative predictor–corrector approach, where in each iteration step the cross-terms are estimated by using the current estimates of the β_n^m, it is possible to eliminate this error for a surprisingly large range of β_n^m. We shall demonstrate these and other points at the end of section 4 by showing results of simulations.

We next describe the contents of section 5. The retrieval methods of sections 3 and 4 are valid for the cases that the numerical aperture NA is not too large, say ≤ 0.60, and that the illumination source can truly be considered as a delta function. When NA is very high, say beyond 0.80, a scalar treatment of the point-spread function as we have it here is not adequate anymore, and also the state of polarization has to be taken into account. Such an effort has been undertaken in [29] for the forward problem and is underway for the inverse problem in [30]; the computational schemes get quite complicated. However, in the intermediate range of NA's, see $0.60 \leq \mathrm{NA} \leq 0.80$, when using natural light, the point-spread function can still be adequately represented by the Fourier integral in (4) in which one replaces

$$\exp[\mathrm{i}f\rho^2] \quad \text{by} \quad A_{\mathrm{R}}(\rho) \exp[\mathrm{i}\Phi_C(\rho)], \tag{18}$$

where

$$A_{\mathrm{R}}(\rho) = (1 - \mathrm{NA}^2\rho^2)^{-1/4}, \quad \Phi_C(\rho) = f\frac{1 - (1 - \mathrm{NA}^2\rho^2)^{1/2}}{1 - (1 - \mathrm{NA}^2)^{1/2}}. \tag{19}$$

In (19), A_{R} is an amplitude function accounting for the radiometric effect and Φ_C is the phase function that correctly describes defocusing in the exit pupil. This is consistent with the formulas in [29], sections 3 and 4. Note that $A_{\mathrm{R}}(\rho)$ and $\Phi_C(\rho)$ can be approximated by 1 and $f\rho^2$, respectively, in the low-NA regime.

Our retrieval methods can be adjusted for the substitution in (18) as follows. We determine (near-) optimal complex numbers $\tilde{f}$, $\tilde{g}$ such that

$$A_{\mathrm{R}}(\rho)\,\exp[\mathrm{i}\Phi_C(\rho)] \approx \exp(\tilde{g} + \mathrm{i}\tilde{f}\rho^2), \tag{20}$$

and we replace all

$$V_n^m(r,f\,) \quad \text{by} \quad \exp(\tilde{g})V_n^m(r,\tilde{f}). \tag{21}$$

Here we note that nothing prevents us from using formula (10) for V_n^m with a complex argument f.

In a similar way, we can account for the effect of using our methods with an illumination source of non-negligible radius $a > 0$. Then the pupil function must be multiplied by the Fourier transform, in normalized form $J_1(2\pi a\rho)/\pi a\rho$, of a disc of radius a, where a is expressed in units λ/NA. This $J_1(2\pi a\rho)/\pi a\rho$ admits an accurate approximation as in (20) for values of a as large as 0.4, so that an amplitude drop at the rim of the pupil of some 50% may occur. In section 5 we detail all this, and we present results of simulations that support the claims made above.

Finally, in section 6 we present conclusions and we present a list of other effects that could have been studied by simulations. Section 6 also enumerates a number of fundamental aspects of the methods that should be addressed in the future.

3. Retrieval of pure-phase aberrations

In this section we work out the method as sketched in subsection 1.2, also see [3], for the retrieval of the Zernike coefficients α_n^m of the aberration phase

$$\Phi(\rho,\vartheta) = \sum_{n,m} \alpha_n^m R_n^m(\rho)\cos m\vartheta \tag{22}$$

occurring in the pupil function $P = \exp[\mathrm{i}\Phi]$ from the intensity $I = |U|^2$ in the focal region. Furthermore, we present a number of simulation results to assess the performance of the method.

3.1 *Detailed description of the method*

We linearize $\exp[\mathrm{i}\Phi]$ as in (6) so that the approximation (8) of U results. We assume that we have available measurements I_{meas} of the intensity I in the $(r,\varphi;f\,)$-space, and we intend to estimate the α_n^m by adopting a best-fit approach in (13). A convenient decoupling in subproblems per m occurs by multiplying (13) by $\cos m\varphi$ and averaging over $\varphi \in [0, 2\pi]$. We thus introduce for $m = 0, 1, \ldots$ the functions

$$\Psi^m_{\text{meas}}(r,f\,) = \frac{1}{2\pi}\int_0^{2\pi} I_{\text{meas}}(r,\varphi;f\,)\cos m\varphi\,\mathrm{d}\varphi \tag{23}$$

and

$$\Psi^m_n(r,f\,) = -8\varepsilon_m^{-1}\,\mathrm{Im}\,[\mathrm{i}^m V^m_n(r,f\,)V^{0*}_0(r,f\,)], \tag{24}$$

where $\varepsilon_0 = 1$, $\varepsilon_1 = \varepsilon_2 = \cdots = 2$ (Neumann's symbol). The Ψ^m_{meas} in (23) are obtained from the measured data by a Fourier analysis in which only the cosine part matters for our symmetry assumption. In (24) we restrict to integer $n, m \geq 0$ with $n - m \geq 0$ and even; all V^m_n are analytically available in accordance with (10) and (11). With these notations, we can write (12) under deletion of the term C in (13) as

$$\Psi^m_{\text{meas}}(r,f\,) \approx 4\delta_{mo}|V^0_0(r,f\,)|^2 + \sum_n \alpha^m_n \Psi^m_n(r,f\,), \tag{25}$$

where $m = 0, 1, \ldots$ and where we have used Kronecker's delta δ_{mo}.

Having decoupled per $m = 0, 1, \ldots$, we next choose the α^m_n, $n = m, m+2, \ldots$, such that in (25) the match between the left-hand side data and the (approximate) theoretical expression on the right-hand side is optimized. For this we introduce an inner product for functions $\Psi(r,f\,)$ and $\chi(r,f\,)$ as

$$(\Psi, \chi) = \int_0^\infty \int_{-\infty}^\infty \Psi(r,f\,)\chi^*(r,f\,)r\,\mathrm{d}r\,\mathrm{d}f. \tag{26}$$

Before proceeding we note that

$$(|V^0_0|^2, \Psi^0_{n'}) = 0, \quad \text{all } n'. \tag{27}$$

This follows from the more general fact, see (9), that for all m, n

$$V^m_n(r,-f\,) = V^{m*}_n(r,f\,), \tag{28}$$

so that $|V^0_0|^2$ is even in f while all $\Psi^0_{n'}$ are odd in f. Now taking inner products in (25) we get for $m = 0, 1, \ldots$

$$\sum_n \alpha^m_n(\Psi^m_n, \Psi^m_{n'}) \approx (\Psi^m_{\text{meas}}, \Psi^m_{n'}), \tag{29}$$

in which n, n' are restricted to the range $m, m+2, \ldots$.

For $m = 0, 1, \ldots$ a vector of estimates $\hat{\boldsymbol{\alpha}}^m$ of $\boldsymbol{\alpha}^m = (\alpha^m_n)_{n=m,\,m+2,\ldots}$ can now be obtained from (29) as follows. We define a Gram matrix G^m by

$$G^m = ((\Psi^m_n, \Psi^m_{n'}))_{n',\,n=m,\,m+2,\ldots}, \tag{30}$$

and a right-hand side vector $\mathbf{r}^m$ by

$$\mathbf{r}^m = ((\Psi^m_{\text{meas}}, \Psi^m_{n'}))_{n'=m,\,m+2,\ldots}, \tag{31}$$

and we set

$$\hat{\boldsymbol{\alpha}}^m = (G^m)^{-1}\mathbf{r}^m, \tag{32}$$

where $(G^m)^{-1}$ is the inverse of the Gram matrix G^m in (30). This completes the description of our estimation procedure.

We shall now note particular features of the method just given. It has been observed numerically, also see the simulation results below, that the functions Ψ^m_n,

$n = m, m+2, \ldots$, for fixed $m = 0, 1, \ldots$ are close to being orthogonal with respect to the inner product in (26). As a consequence, the Gram matrices in (30) are well conditioned and the inversions in (32) present no problems.

In a practical implementation of the method, the ranges in (29) for n, n' are finite, say $m, m+2, \ldots, m+2M$. The solution vector $\hat{\boldsymbol{\alpha}}^m(M)$ obtained by solving the truncated system has the property that

$$\left\| \Psi^m_{\text{meas}} - \sum_{n=m,\, m+2,\ldots,\, m+2M} \eta^m_n \Psi^m_n \right\|^2 \tag{33}$$

is minimal for $\eta^m_n = \hat{\alpha}^m_n(M)$, $n = m, m+2, \ldots, m+2M$. Here $\| \ \|$ is the inner product norm corresponding to $(,)$ in (26).

A second finitization aspect is the truncation and discretization of the integrals over r and f. We have observed that the condition numbers of the Gram matrices quickly saturate at their limiting values when we take evenly spaced f's in a symmetric range contained in $[-4\pi, 4\pi]$ and r's that cover a range $[0, (m+2M+5)/2\pi]$ when G^m is truncated as above. One should think here of 9–15 f-samples and 512 r-samples. Note that choosing the f range finite but symmetric around 0 maintains orthogonality of $|V^0_0|^2$ and $\Psi^0_{n'}$, see (27).

We next assess the effect of linearization of $\exp[\mathrm{i}\Phi]$ in (6) and deletion of the term (13) in the linear systems of (29). We start with the second issue, and we shall show that (13) vanishes altogether when we multiply by $\cos m\varphi$ and average over $\varphi \in [0, 2\pi]$ and, subsequently, take inner products with the $\Psi^m_{n'}$. As a result, we have that the system of equations in (29) would have resulted as well when we would have worked with an intensity in which the term (13) were included. To prove this claim, we first observe that multiplying (13) by $\cos m\varphi$ and averaging over $\varphi \in [0, 2\pi]$ causes all terms to vanish with indices m_1, m_2 such that $|m_1 \pm m_2| \neq m$. Thus there remains

$$\mathrm{Re}\,[\mathrm{i}^{m_1 - m_2} V^{m_1}_{n_1}(r, f\,) V^{m_2 *}_{n_2}(r, f\,)] \tag{34}$$

with $|m_1 \pm m_2| = m$. We get from (28) that the function in (34) is even in f when m is even and odd in f when m is odd. Similarly, it follows from (28) that the function $\Psi^m_{n'}(r, f\,)$ in (24) is odd in f when m is even and even in f when m is odd. Hence, the functions in (34) with $|m_1 \pm m_2| = m$ and the $\Psi^m_{n'}$ have opposite parity with respect to their dependence on f and, so, their inner products vanish.

We next show that a cancellation as above also occurs for the deleted second-order term $-(1/2)\Phi^2$ in the linearization (6) of $\exp[\mathrm{i}\Phi]$. This second-order term has a contribution U_2 to the true U at the right-hand side of (8) given by

$$U_2(r, \varphi; f\,) = \frac{-1}{2\pi} \int_0^1 \int_0^{2\pi} \exp(\mathrm{i} f \rho^2) \Phi^2(\rho, \vartheta) \exp[2\pi \mathrm{i} \rho r \cos(\vartheta - \varphi)] \rho \, \mathrm{d}\rho \, \mathrm{d}\vartheta. \tag{35}$$

To second order, this U_2 yields a contribution $4\,\mathrm{Re}\,[U_2 V^{0*}_0]$ to the true I at the right-hand side of (13). With Φ given by its Zernike cosine expansion in (21), we get that U_2 is a quadruple series containing terms

$$^{\pm} V^{m_1 m_2}_{n_1 n_2}(r, f\,) \mathrm{i}^{|m_1 \pm m_2|} \cos |m_1 \pm m_2| \varphi, \tag{36}$$

where

$$^{\pm}V_{n_1 n_2}^{m_1 m_2}(r,f\,) = \int_0^1 \rho\, \exp(\mathrm{i}f\rho^2) R_{n_1}^{m_1}(\rho) R_{n_2}^{m_2}(\rho) J_{|m_1 \pm m_2|}(2\pi r\rho)\, \mathrm{d}\rho. \tag{37}$$

For these $^{\pm}V$ the symmetry relation (28) holds equally well. When we multiply U_2 by $\cos m\varphi$ and average over $\varphi \in [0, 2\pi]$, all terms (36) cancel, except those with $|m_1 \pm m_2| = m$. Due to the factors $\mathrm{i}^{|m_1 \pm m_2|}$ in (36) and the symmetry relations holding for V_0^0 and $^{\pm}V$, we see that

$$\frac{1}{2\pi}\int_0^{2\pi} \mathrm{Re}\,[U_2(r,\varphi;f\,) V_0^{0*}(r,f\,)]\, \cos m\varphi\, \mathrm{d}\varphi \tag{38}$$

is even in f when m is even and odd in f when m is odd. Hence the $\Psi_{n'}^m$ and (38) have opposite parity as a function of f, and their inner products vanish. As a result we have that linearization of $\exp[i\Phi]$ as in (6) causes only third- and higher-order errors in the near-identities in (29).

3.2 *Simulations*

(a) In figure 2(*a*) and (*b*), we display the condition numbers of the Gram matrices G^m in (30) (vertical axis in natural logarithms) as a function of the sampling range and density in the focal and radial direction, respectively. These condition numbers are defined as the ratio of the minimum and maximum eigenvalue of the truncated and scaled Gram matrix

$$G_{M,\,\mathrm{scaled}}^m = \left(\frac{(\Psi_n^m, \Psi_{n'}^m)}{\|\Psi_n^m\| \|\Psi_{n'}^m\|} \right)_{n,\,n' = m,\,m+2,\ldots,\,m+2M}, \tag{39}$$

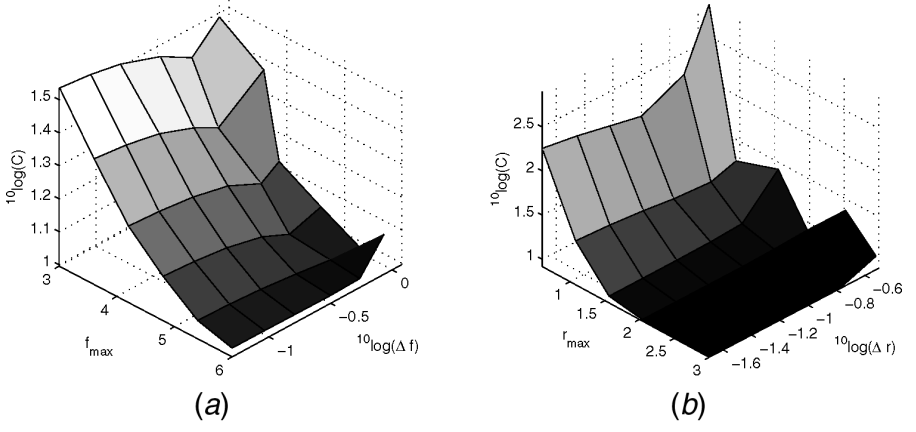

Figure 2. The condition numbers of the Gram matrices are lower when (*a*) the focal range is either extended and/or sampled more densely and (*b*) the radial range is extended and/or sampled more densely. The shown condition numbers are the maxima obtained when considering all truncated and scaled matrices $G_{M,\,\mathrm{scaled}}^m$ in (43) with $m \leq 6,\ m + 2M \leq 10$.

Table 1. Perfect reconstruction.

n	m	α	α_{rec}
2	0	0.3000	0.3000
4	0	0	−0.0000
6	0	0	−0.0000
1	1	0.1000	0.1000
3	1	0.4000	0.4000
5	1	0	−0.0000
2	2	0.2000	0.2000
4	2	0	0.0000
6	2	0	−0.0000
3	3	0	0.0000
5	3	0	0.0000

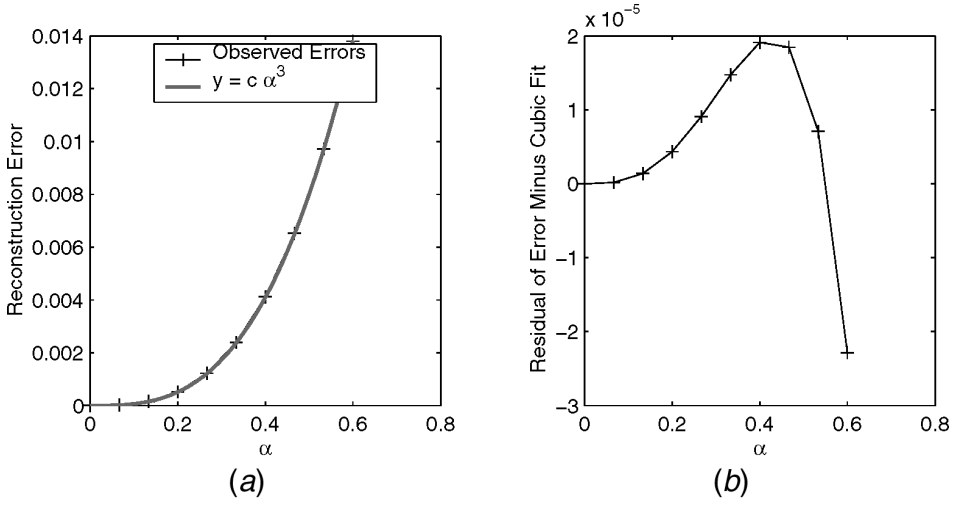

Figure 3. (*a*) The error in the retrieval of the coma coefficient α_3^1 as a function of its size. (*b*) The residual after subtraction of the third-order fit. The scaling parameter c equals 0.0640.

where $\|\Psi\| = (\Psi, \Psi)^{1/2}$. The maximum occurring condition number of all truncated matrices $G^m_{M,\text{scaled}}$ in (39) with $m + 2M \leq 10$, $m \leq 6$ is plotted against the discretization at which the inner products Ψ were calculated. As expected, lower condition numbers occur when a larger focus range is taken and/or more focal planes are used to approximate the inner products of the Ψ^m_n. A similar thing happens for the sampling in the radial direction. The sampling density in the ϑ direction was not found to have much influence on the condition number. It is understood here that the general sampling theorem of taking at least $2m_{\max}$ values of ϑ into account has to be obeyed.

In all further experiments we use (unless stated otherwise)

$$\begin{cases} 11 & f\text{-points equally spaced in } [-2\pi, 2\pi], \\ 64 & \vartheta\text{-points } 2\pi\dfrac{k}{64}, k = 0, 1, \ldots, 63, \\ 512 & r\text{-points equally spaced in } [0, 10/\pi] \end{cases} . \tag{40}$$

This results in Gram matrices (39) having condition numbers of the order of 10 or less.

(b) In table 1 we show that perfect reconstruction occurs for pupil functions P of the form $1 + \mathrm{i}\sum_{n,m} \alpha_n^m Z_n^m$ with *real* α's, finitely many of them $\neq 0$.

(c) In figure 3(*a*) and (*b*), we show that third- and higher-order errors occur in retrieval of α in the comatic pupil function $\exp[\mathrm{i}\alpha Z_3^1(\rho, \vartheta)]$. We have simulated the measured intensity as

$$I_{\text{meas}} = \left| 2 \sum_{n,m} \mathrm{i}^m {}_3^1\beta_n^m(\alpha) V_n^m(r, f\ ) \cos m\varphi \right|^2 , \tag{41}$$

where ${}_3^1\beta_n^m(\alpha)$ are the Zernike coefficients of $\exp[\mathrm{i}\alpha Z_3^1(\rho, \vartheta)]$ as given in the appendix, (A 18), and where the summation extends over all relevant m, n with $m \leq 3, n \leq 6$. In retrieving α it is enough to concentrate on the system (29) with $m = 1$, for which $n, n' = 1, 3, 5$. The observed reconstruction error is

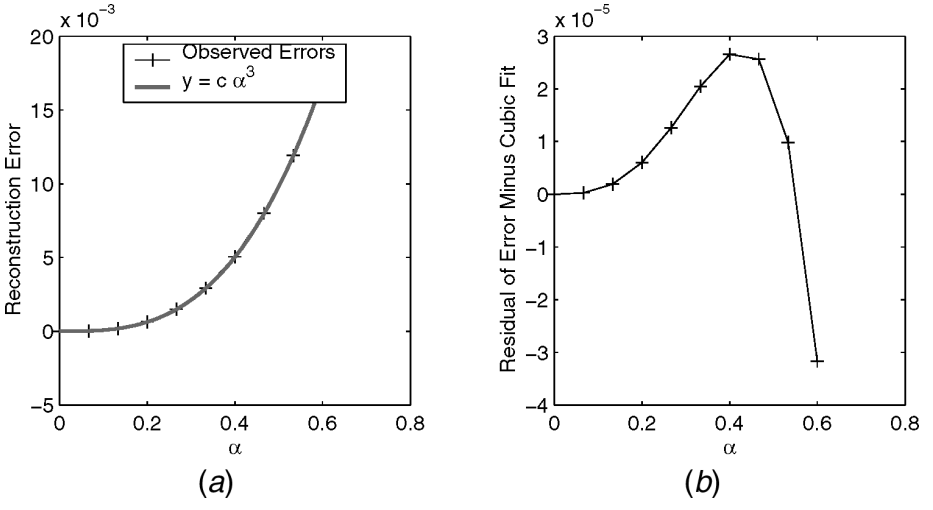

Figure 4. (*a*) The error in the retrieval of the spherical aberration coefficient α_4^0 as a function of its size. (*b*) The residual after subtraction of the third-order fit. The scaling parameter c equals 0.0785.

very accurately described by the third degree polynomial $c\alpha^3$; compare the vertical axes in figure 3(*a*) and (*b*).

A similar exercise was done for retrieval of α in the spherical aberrated pupil function $\exp[\mathrm{i}\alpha Z_4^0(\rho, \vartheta)]$. To simulate the measured intensity, we use the quantities ${}_4^0\beta_{4r}^0(\alpha)$ as given in the appendix with (A 11) and (A 12) so that

Table 2. Effect of adding DC-free noise to the measurement.

n	m	α	$SNR=\infty$ α_{rec}	$SNR=100$ α_{rec}	$SNR=10$ α_{rec}
2	0	0.3000	0.3000	0.2996	0.2989
1	1	0.1000	0.1000	0.1003	0.1027
3	1	0.4000	0.4000	0.4002	0.4082
2	2	0.2000	0.2000	0.1991	0.2087

Table 3. Reconstruction of α's with 41 focal levels, $SNR=2$.

n	m	α	α_{rec}
2	0	0.3000	0.2992
4	0	0	−0.0420
6	0	0	−0.0077
1	1	0.1000	0.0694
3	1	0.4000	0.3688
5	1	0	−0.0233
2	2	0.2000	0.1743
4	2	0	0.0369
6	2	0	−0.0278
3	3	0	−0.0147
5	3	0	0.0315

$$I_{\text{meas}} = \left| 2 \sum_r {}^0_4\beta^0_{4r}(\alpha) V^0_{4r} \right|^2, \tag{42}$$

where $r = 0, 1, 2, 3, 4$. In retrieving α, we concentrate on the system (29) with $m=0$ and $n, n' = 2, 4, \ldots, 16$. Again, a third-order monomial describes the reconstruction error accurately. See figure 4(*a*) and (*b*).

(d) We consider next the effect of adding DC-free noise to the measured intensities. Although this leads to locally negative intensities, which may seem unrealistic, it is in an experimental setting with noise present necessary to subtract a DC offset from the measured intensity so as to avoid severe errors when solving the system (29) with $m=0$. This DC offset is estimated as the average intensity value present in the best focus plane ($f=0$) far outside the Airy disc. In table 2 we display reconstruction results for a case as in (b) above where we have added Gaussian DC-free noise with $SNR = \infty, 100, 10$ and with the standard sampling scheme (40) in effect. Increasing the number of focal planes from 11 to 41 shows that even for SNR as low as 2, fair reconstruction results are still possible (table 3).

In figure 5(*a*)–(*c*) the influence of addition of Gaussian DC-free noise on the third-order behaviour of the reconstruction error for a comatic pupil function $\exp[\mathrm{i}\alpha Z^1_3]$ is shown with $SNR=\infty$ (compare with figure 3(*a*)), 100, 10. We see that the cubic law continues to be in force, though with varying proportionality constants.

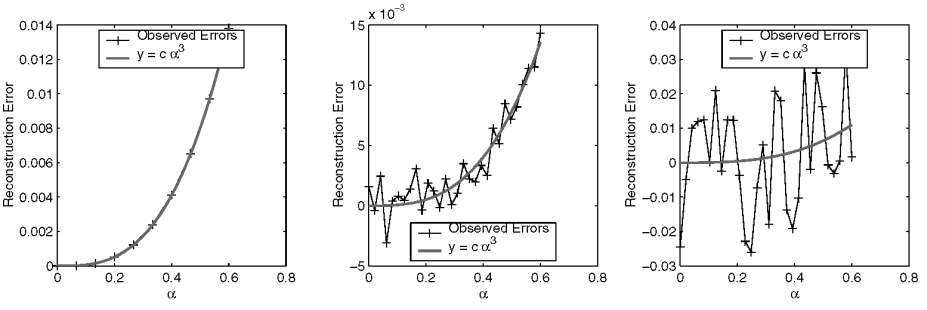

(*a*) $SNR = \infty$ $c = 0.0089$ (*b*) $SNR = 100$ $c = 0.0628$ (*c*) $SNR = 10$ $c = 0.0509$

Figure 5. The reconstruction error of the coma coefficient is related in third-order to the size of the true aberration present, even in the presence of noise in the measured data.

4. Retrieval of general aberrations

In section 3 we have considered the problem of retrieving the phase Φ of a pupil function $P = \exp[i\Phi]$ with a pure-phase aberration. The resulting algorithm is surprisingly simple and easy to implement, yields accurate results in practice [7], and can be used in the case where it is safe to ignore third-order terms $-i\Phi^3/6$. However, its application range is restricted to pure-phase aberrations. In this section we present a method for retrieving both amplitude $A > 0$ and phase Φ of a pupil function $P = A\exp[i\Phi]$ from the intensity point-spread function in the focal region. Furthermore, we present a number of simulation results to assess the performance of the method.

4.1 *Detailed description of the method*

We start by expanding the pupil function P into a Zernike cosine series

$$P = A\exp[i\Phi] = \sum_{n,m} \beta_n^m Z_n^m; \quad Z_n^m(\rho,\vartheta) = R_n^m(\rho)\cos m\vartheta, \tag{43}$$

where now the β_n^m are general complex numbers. In the often occurring case that $A \approx 1$, Φ small, we have that $\beta_0^0 \approx 1$ while all other β_n^m are small, and in that case the imaginary parts of the β_n^m describe Φ (pretty much as the α_n^m of section 3 did) while the real part of the β_n^m describes $\ln A$. When $A \not\approx 1$ and/or Φ is not small, the physical significance of the β's is not straightforward anymore, but this diminishes in no way the efficiency of the representation of P by means of its Zernike coefficients.

We assume that β_0^0 is positive and relatively large compared to the other β_n^m's; the positivity assumption may be made, since we observe intensities, and we can retrieve the coefficients only up to an overall phase factor. We obtain for the point-spread function from (43) the exact representation

$$U(r,\varphi;f) = 2\beta_0^0 V_0^0(r,f) + 2{\sum_{n,m}}' \beta_n^m i^m V_n^m(r,f)\cos m\varphi, \tag{44}$$

where the $'$ on the summation sign denotes that the term with $n = m = 0$ has been deleted. Expanding $I = |U|^2$, we obtain

$$I \approx 4(\beta_0^0)^2 |V_0^0|^2 + 8 \sum_{n,m}{}' \beta_0^0 \operatorname{Re}(\beta_n^m) \operatorname{Re}[\mathrm{i}^m V_n^m V_0^{0*}] \cos m\varphi$$
$$- 8 \sum_{n,m}{}' \beta_0^0 \operatorname{Im}(\beta_n^m) \operatorname{Im}[\mathrm{i}^m V_n^m V_0^{0*}] \cos m\varphi. \tag{45}$$

Here we have omitted the term

$$4 \sum_{n_1,m_1;n_2,m_2}{}'' \operatorname{Re}[\beta_{n_1}^{m_1} \beta_{n_2}^{m_2 *} \mathrm{i}^{m_1 - m_2} V_{n_1}^{m_1} V_{n_2}^{m_2 *}] \cos m_1\varphi \cos m_2\varphi, \tag{46}$$

where the $''$ on the summation sign denotes that all terms with $n_1 = m_1 = 0$ or $n_2 = m_2 = 0$ have been deleted.

We next proceed as in section 3 by introducing, along with the functions Ψ_n^m in (24) appearing on the second line of (45), the functions

$$\chi_n^m(r,f\,) = 8\varepsilon_m^{-1} \operatorname{Re}[\mathrm{i}^m V_n^m(r,f\,) V_0^{0*}(r,f\,)] \tag{47}$$

with ε_m Neumann's symbol as in (24). Furthermore, we let Ψ_{meas}^m as in (23). Then, upon multiplying the near-identity in (45) by $\cos m\varphi$ and averaging over $\varphi \in [0, 2\pi]$, we get

$$\Psi_{\mathrm{meas}}^0 \approx \frac{1}{2}(\beta_0^0)^2 \chi_0^0 + \sum_n{}' \beta_0^0 \operatorname{Re}(\beta_n^0) \chi_n^0 + \sum_n{}' \beta_0^0 \operatorname{Im}(\beta_n^0) \Psi_n^0, \tag{48}$$

$$\Psi_{\mathrm{meas}}^m \approx \sum_n \beta_0^0 \operatorname{Re}(\beta_n^m) \chi_n^m + \sum_n \beta_0^0 \operatorname{Im}(\beta_n^m) \Psi_n^m, \tag{49}$$

for $m = 0$ and $m = 1, 2, \ldots$, respectively.

We shall now take inner products as in section 3 where we note the following consequence of (28): for all $m = 0, 1, \ldots$ we have

$$(\chi_n^m, \Psi_{n'}^m) = 0, \quad \text{all } n, n' = m, m+2, \ldots. \tag{50}$$

Indeed, it follows from (28) that χ_n^m is even in f when m is even and odd in f when m is odd, whereas $\Psi_{n'}^m$ is odd in f when m is even and even in f when m is odd. Hence, building for $m = 0, 1, \ldots$ linear systems as in (29) by taking inner products in the near-identities in (45) and (46) with $\chi_{n'}^m$, $\Psi_{n'}^m$, we get a decoupling according to

$$\begin{cases} \frac{1}{2}(\beta_0^0)^2 (\chi_0^0, \chi_{n'}^0) + \sum_n{}' \beta_0^0 \operatorname{Re}(\beta_n^0)(\chi_n^0, \chi_{n'}^0) \approx (\Psi_{\mathrm{meas}}^0, \chi_{n'}^0), \\ \sum_n{}' \beta_0^0 \operatorname{Im}(\beta_n^0)(\Psi_n^0, \Psi_{n'}^0) \approx (\Psi_{\mathrm{meas}}^0, \Psi_{n'}^0) \end{cases} \tag{51}$$

for $m = 0$ where $n, n' = 0, 2, \ldots$, and

$$\begin{cases} \sum_n \beta_0^0 \operatorname{Re}(\beta_n^m)(\chi_n^m, \chi_{n'}^m) \approx (\Psi_{\mathrm{meas}}^m, \chi_{n'}^m), \\ \sum_n \beta_0^0 \operatorname{Im}(\beta_n^m)(\Psi_n^m, \Psi_{n'}^m) \approx (\Psi_{\mathrm{meas}}^m, \Psi_{n'}^m) \end{cases} \tag{52}$$

for $m = 1, 2, \ldots$ where $n, n' = m, m+2, \ldots$.

The procedure to estimate the β_n^m's is now as follows. We solve the first system in (51) involving $(\beta_0^0)^2$, $\beta_0^0 \operatorname{Re}(\beta_n^0)$ linearly. This then gives β_0^0 (which was assumed to be positive) and subsequently $\operatorname{Re}(\beta_n^0)$, $n = 2, 4, \ldots$. Having found β_0^0, we can now solve the second system in (51) involving $\beta_0^0 \operatorname{Im}(\beta_n^0)$ linearly and the two systems in (52) involving $\beta_0^0 \operatorname{Re}(\beta_n^m)$ and $\beta_0^0 \operatorname{Im}(\beta_n^m)$, respectively, linearly for $m = 1, 2, \ldots$. We thus obtain estimates $\hat{\beta}_n^m$ by replacing all $\approx$ in (51) and (52) by $=$ and solving the linear systems.

Note that in the case of purely imaginary β_n^m, only the second lines in (51) and (52) need to be considered (and also the first line in (51) with $n' = 0$ to find β_0^0). This then yields the pure-phase retrieval method of section 3.

As in the case of pure-phase retrieval, the systems are normally well conditioned since either system $(\Psi_n^m)_{n=m,\,m+2,\ldots}$ and $(\chi_n^m)_{n=m,\,m+2,\ldots}$ is close to being orthogonal. Also, the finitization issues are similar to those in the pure-phase retrieval case.

However, the deletion of the small cross-terms expression (46) from the theoretical intensity $I = |U|^2$ has a quite different effect on the linear systems in (51) and (52) than the deletion of (13) had on the systems in (29). The reason for this is that the functions

$$\operatorname{Re}[\beta_{n_1}^{m_1} \beta_{n_2}^{m_2 *} \mathrm{i}^{m_1 - m_2} V_{n_1}^{m_1} V_{n_2}^{m_2 *}] \tag{53}$$

are, in general, neither even nor odd in f since the β_n^m are general complex numbers.

A simple predictor–corrector approach, however, can eliminate the error incurred by deleting the term in (46) in many cases completely. Here one constructs iteratively estimates $\hat{\beta}_n^m(k)$ of the β_n^m as follows. We let $\hat{\beta}_n^m(0) = \hat{\beta}_n^m$, where $\hat{\beta}_n^m$ are the estimates of β_n^m as found by applying the above procedure in which the $\approx$ in (51) and (52) are replaced by $=$. Having $\hat{\beta}_n^m(k)$ available for some $k = 0, 1, \ldots$, we apply the above procedure for finding $\hat{\beta}_n^m$, however, with the measured I_{meas} replaced with $I_{\text{meas}} - E(k)$ in which $E(k)$ is the term (46) with

$$\hat{\beta}_{n_1}^{m_1}(k)(\hat{\beta}_{n_2}^{m_2}(k))^* \text{ substituted for } \beta_{n_1}^{m_1}(\beta_{n_2}^{m_2})^*. \tag{54}$$

Under normal conditions, this predictor–corrector procedure converges rapidly while even under not so favourable conditions (with β_0^0 not large or even rather small compared to some of the other β_n^m) convergence, be it slow, often takes place as well.

The computational scheme for the predictor–corrector approach requires handling the quantities $I_{\text{meas}} - E(k)$, $k = 0, 1, \ldots$, as if they were measured quantities. Thus these $I - E(k)$ have to be multiplied by $\cos m\varphi$ and averaged over $\varphi \in [0, 2\pi]$, and, subsequently, inner products with the $\chi_{n'}^m$, $\Psi_{n'}^m$ have to be taken. Because of the special form of the $E(k)$, see (46), and the symmetry properties of the terms in (46), see (28), this can be done in a considerably more efficient way, but we shall not present the details here since the administration is rather involved.

4.2 *Simulations*

(a) In figure 6(*a*)–(*c*) we show that second-order reconstruction errors occur in the case that the pupil function P is given as $P = 1 + \beta_4^0 R_4^0$, where β_4^0 is real.

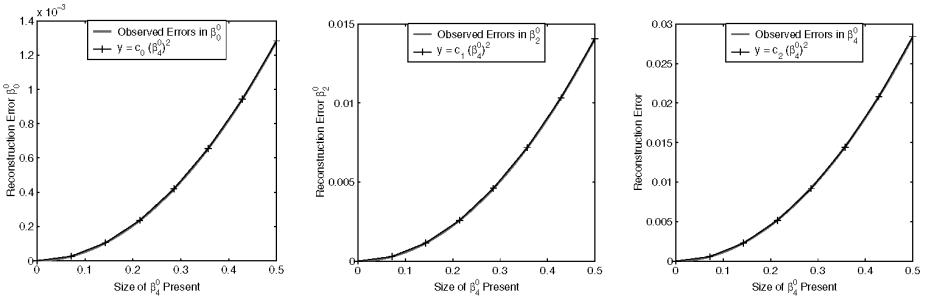

(*a*) $c_0 = 0.0051$ (*b*) $c_1 = 0.0563$ (*c*) $c_2 = 0.1133$

Figure 6. Quadratic dependence of the reconstruction errors on the size of the aberration present: (*a*) $|1 - \hat{\beta}_0^0|$, (*b*) $|0 - \hat{\beta}_2^0|$, (*c*) $|\beta_4^0 - \hat{\beta}_4^0|$.

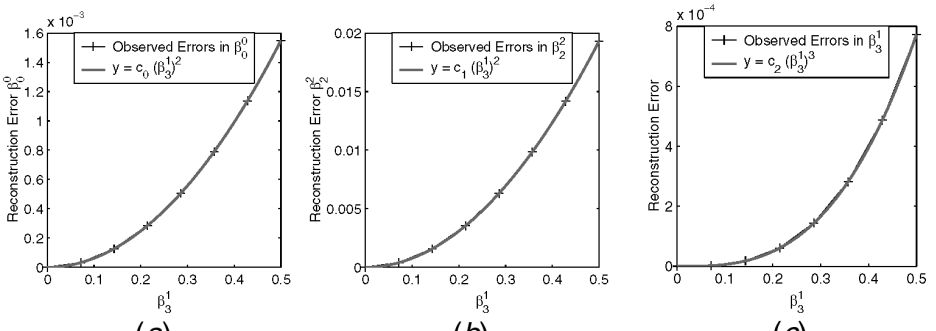

(*a*) $c_0 = 0.0062$ (*b*) $c_1 = 0.0772$ (*c*) $c_2 = 0.0062$

Figure 7. Quadratic dependence of the reconstruction errors on the size of the aberration present: (*a*) $|1 - \hat{\beta}_0^0|$, (*b*) $|0 - \hat{\beta}_2^2|$. Cubic dependence for the reconstruction error of the aberration that was present: (*c*) $|\beta_3^1 - \hat{\beta}_3^1|$.

We now use $I_{\text{meas}} = |2V_0^0 + 2V_4^0|^2$, and it is sufficient to consider the first system in (51). The deleted small second-order term involving $(\beta_4^0)^2$ causes $|1 - \hat{\beta}_0^0|$ to behave quadratically, and similarly for $|0 - \hat{\beta}_2^0|$ and $|\beta_4^0 - \hat{\beta}_4^0|$.

A similar exercise has been done with the pupil function $P = 1 + \beta_3^1 Z_3^1$ with real β_3^1. Now the first system in (51) and the first systems in (52) with $m = 1, 2$ should be considered (the other systems are trivial). The deleted small second-order term involving $(\beta_3^1)^2$ has an impact on the first system in (51) and the system in (52) with $m = 2$. Consequently, we have that $|1 - \hat{\beta}_0^0|$ behaves quadratically and so does $|0 - \hat{\beta}_2^2|$. The reconstruction error $|\beta_3^1 - \hat{\beta}_3^1|$ behaves cubically. This latter fact can be explained from the circumstance that the first system in (52) with $m = 1$ (from which $\beta_0^0 \beta_3^1$ is estimated) has only the term $\beta_0^0 \beta_3^1 (\chi_3^1, \chi_{n'}^1)$ on the left-hand side, whence the second-order error in $\hat{\beta}_0^0$ produces a third-order error in $\hat{\beta}_3^1$. See figure 7(*a*)–(*c*).

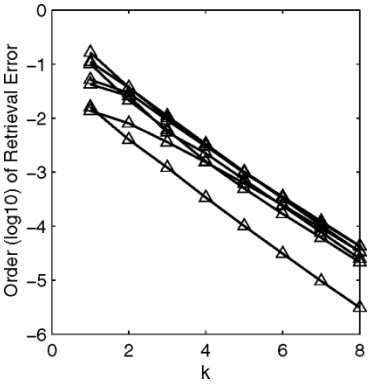

Figure 8. The absolute values of the reconstruction errors drop about 5 dB in each iteration of the predictor–corrector method.

Table 4. Present aberration coefficients.

$\beta_0^0 = 1$	$\beta_1^1 = 0.1 - 0.3\mathrm{i}$	$\beta_2^2 = 0.5 + 0.2\mathrm{i}$
$\beta_2^0 = -0.2 - 0.1\mathrm{i}$	$\beta_3^1 = -0.4 + 0.4\mathrm{i}$	$\beta_4^2 = 0.5 + 0.6\mathrm{i}$
$\beta_4^0 = 0.3 + 0.6\mathrm{i}$		

(b) We consider here and in (c) and (d) below the predictor–corrector method. We first consider the case that the pupil function P is given exactly as $\sum_{n,m} \beta_n^m Z_n^m$ with finitely many $\beta_n^m \neq 0$ and $|\beta_n^m| < \beta_0^0$, β_n^m complex. The measured intensity is then $|2\sum_{n,m} \mathrm{i}^m \beta_n^m V_n^m(r,f)\cos m\varphi|^2$ and the linear systems in (51) and (52) involve all $m \leq$ (two times largest m with $\beta_n^m \neq 0$ for some n) and all $n, n' \leq$ (two times largest n with $\beta_n^m \neq 0$ for some m). Figure 8 displays the reconstruction errors $|\beta_n^m - \hat{\beta}_n^m(k)|$ as a function of the number of iterations for all those n, m with $\beta_n^m \neq 0$, see table 4 for these β_n^m. There are also several (non-displayed) curves of spurious $|\hat{\beta}_n^m(k)|$ corresponding to m, n for which $\beta_n^m = 0$.

In figure 9 we consider for the example of table 4 the real and imaginary parts of the specific convergence histories of the $\hat{\beta}_n^m(k)$ with $\beta_n^m \neq 0$. We conclude from both figures 8 and 9 that there is rapid convergence.

It is also interesting to consider a case where some of the $|\beta_n^m|$ are allowed to be larger than β_0^0, see table 5. These β_n^m are obtained as the quantities $\frac{1}{3}\beta_n^m(\alpha)$ of the appendix, (A 18), of the comatic pupil function $\exp[\mathrm{i}\alpha Z_3^1]$ with α as large as $2(1.6)^{1/2}$ (twice the diffraction limit) and $n \leq 6$, $m \leq 3$. Evidently, for accurately representing $\exp[\mathrm{i}\alpha Z_3^1]$ where α is this large, considerably more terms should be considered; however, our present intention is just to show that perfect reconstruction is possible with the non-dominant β_0^0 term, and taking $\exp[\mathrm{i}\alpha Z_3^1]$ with large α is such a case. The 4th and 6th columns show reconstruction results after 100 iterations. In figure 10 we display the

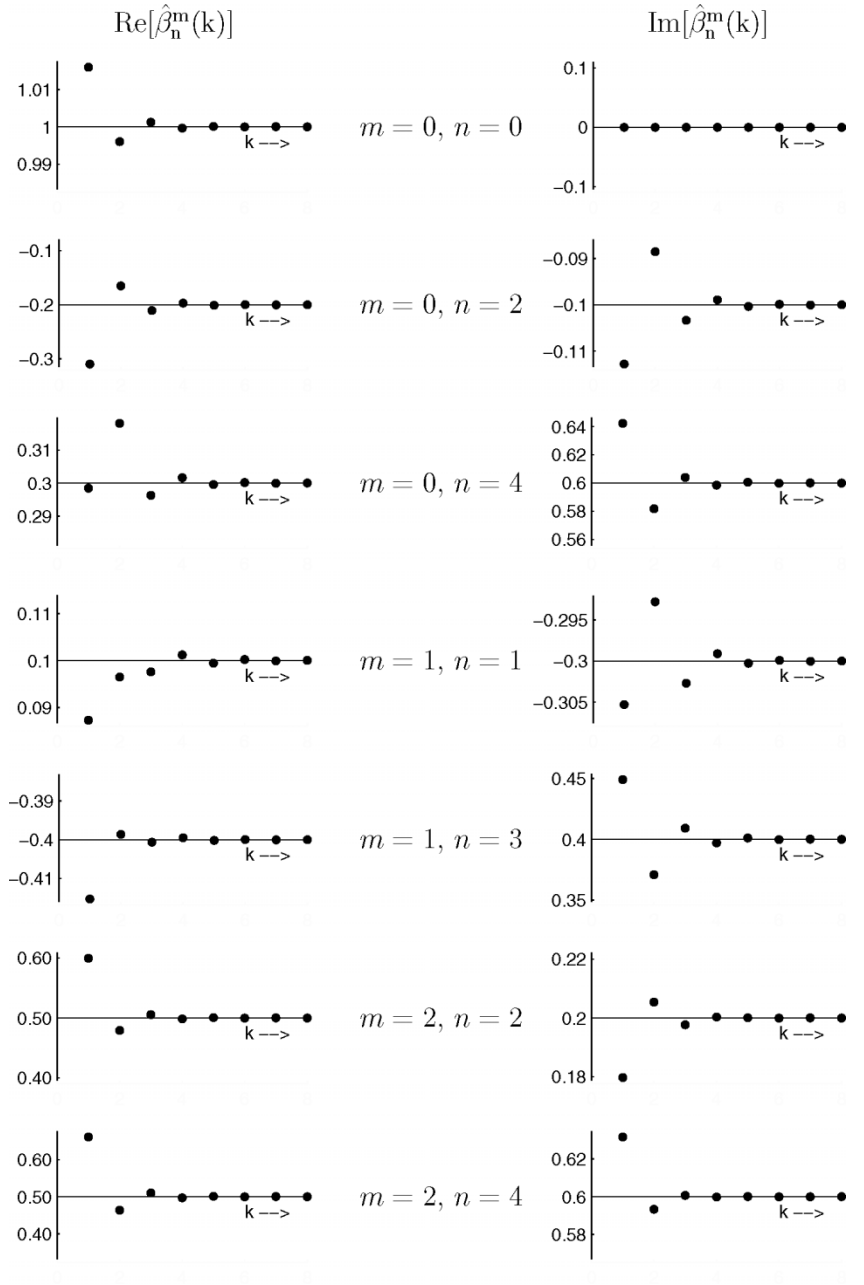

Figure 9. Successive values of real and imaginary parts of $\hat{\beta}^m_n(k)$, $k = 0, 1, \ldots, 7$ for the example of table 4. The horizontal axes are positioned on the values given through the table.

Table 5. Applied and retrieved (100 iterations) aberration coefficients.

n	m	$\mathrm{Re}(\beta)$	$\mathrm{Re}(\hat{\beta})$	$\mathrm{Im}(\beta)$	$\mathrm{Im}(\hat{\beta})$
0	0	0.6610	0.6611	0	0
2	0	−0.0303	−0.0312	0	−0.0000
4	0	−0.2875	−0.2869	0	0.0000
6	0	−0.5506	−0.5502	0	−0.0000
1	1	0	0.0000	−0.1007	−0.1006
3	1	0	−0.0000	1.7948	1.7924
5	1	0	−0.0000	−0.1867	−0.1858
2	2	−0.4872	−0.4857	0	0.0000
4	2	0.0852	0.0876	0	−0.0000
6	2	−0.6983	−0.6991	0	−0.0000
3	3	0	−0.0000	−0.1134	−0.1125
5	3	0	0.0000	−0.2385	−0.2376

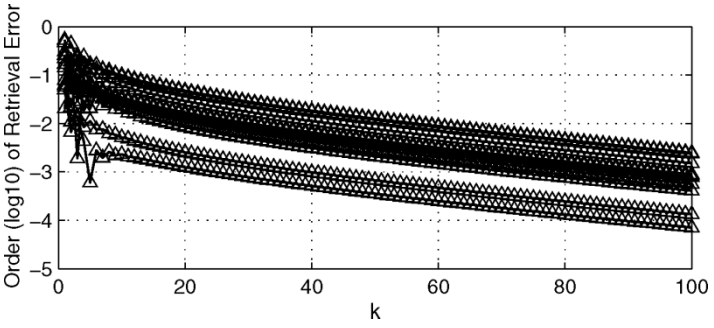

Figure 10. The absolute values of the reconstruction errors $|\beta_n^m - \hat{\beta}_n^m(k)|$ decrease slowly but steadily for $\alpha = 2(1.6)^{1/2}$. The largest error after 100 iterations (k) is below $10^{-2.5}$.

reconstruction error curves $|\beta_n^m - \hat{\beta}_n^m(k)|$ for n, m as in table 5 which occur with $\beta_n^m \neq 0$. Indeed, convergence takes place, but at a very slow rate.

A similar example, with $\alpha = 5$, shows clear divergence of the predictor–corrector method.

(c) The potential of perfect reconstruction using the predictor–corrector approach can also be demonstrated on the level of pupil functions. We consider the pupil function

$$P(\rho, \vartheta) = \exp\left[-\delta\rho^2 + \mathrm{i}\alpha Z_3^1(\rho, \vartheta)\right] \tag{55}$$

(Gaussian amplitude with $\delta = 0.2$, comatic phase function with $\alpha = 0.2$). Using the fact that the V_n^m-functions in (9) and (10) can be evaluated with complex focal arguments as well, we have for the measured intensity the representation

$$I_{\mathrm{meas}} = \left| 2 \sum_{n,m} \mathrm{i}^{m} {}_3^1\beta_n^m(\alpha) V_n^m(r, f + \mathrm{i}\delta) \cos m\varphi \right|^2, \tag{56}$$

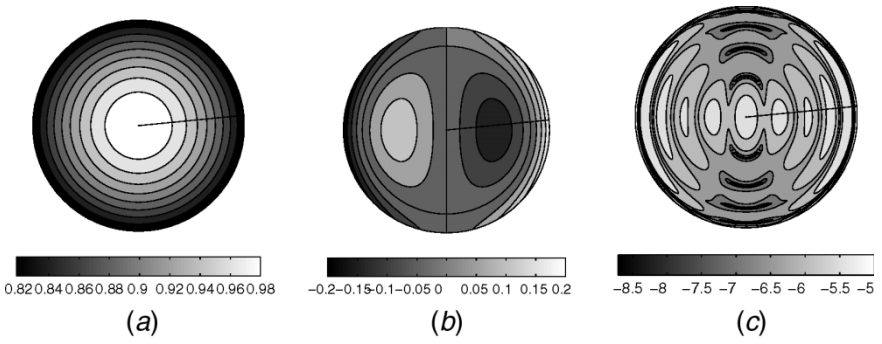

Figure 11. The pupil function $P(\rho, \vartheta)$ to be retrieved is (*a*) a Gaussian transmission (*b*) together with a comatic phase. (*c*) The absolute reconstruction error $|P(\rho, \vartheta) - P_{\text{rec}}(\rho, \vartheta)|$ is displayed in grey-scale coded powers of 10.

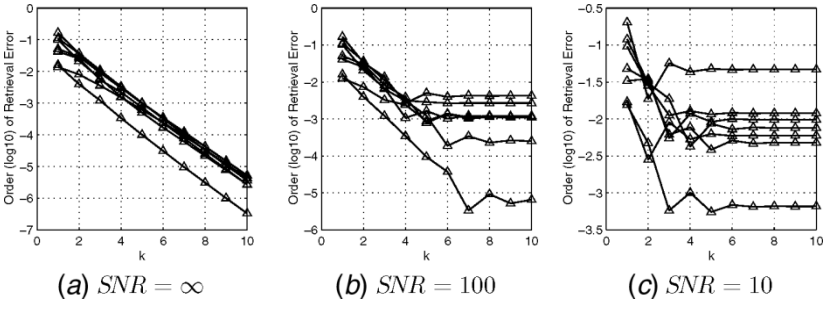

Figure 12. The performance of the predictor–corrector approach is demonstrated in the presence of noise. The aberrations to be retrieved are listed in table 4 and the reconstruction errors $|\beta_n^m - \hat{\beta}_n^m(k)|$ are plotted at each iteration $k = 1, \ldots, 10$ for the cases $SNR = \infty, 100, 10$ in (*a*), (*b*) and (*c*) respectively. The presence of noise in the measurement imposes a limit to the convergence of the predictor–corrector approach.

where $\frac{1}{3}\beta_n^m(\alpha)$ are as in the appendix, (A 18), and the summation extends over all relevant m, n with $m \leq 4, n \leq 8$. In figure 11, we display the reconstruction error $|P(\rho, \vartheta) - P_{\text{rec}}(\rho, \vartheta)|$ where

$$P_{\text{rec}}(\rho, \vartheta) = \sum_{n,m} \beta_{n,\text{rec}}^m Z_n^m(\rho, \vartheta) \tag{57}$$

and $\beta_{n,\text{rec}}^m$ are obtained as $\beta_n^m(k)$ with iteration number $k = 8$.

(d) It is, furthermore, interesting to see how the predictor–corrector method performs in the presence of (Gaussian) DC-free noise. We use the same (non-zero) β_n^m's as in table 4 and in figure 12(*a*)–(*c*) we show the convergence history (using 10 iterations) of the various $\hat{\beta}_n^m(k)$ for the cases where $SNR = \infty, 100, 10$, respectively; the graphs display the reconstruction errors $|\beta_n^m - \hat{\beta}_n^m(k)|$ for those m, n that have $\beta_n^m \neq 0$. In the above example we have

$|\beta_n^m| < \beta_0^0 = 1$, but we also have examples with some $|\beta_n^m|$ (considerably) larger than β_0^0 with good results. From the plots in figure 12(*a*)–(*c*) it is seen that the reconstruction errors saturate at a certain level depending clearly on the *SNR*. We also have observed that increasing sample densities has a beneficial effect on the saturation levels of the reconstruction errors.

5. Extension of the method

The methods for retrieval of the aberration coefficients presented in sections 3 and 4 assume relatively low NA and use of an illumination source of very small lateral size so that the pupil is uniformly illuminated. For higher values of NA (≥ 0.60), the conventional approximation $\exp[\mathrm{i}f\rho^2]$, describing defocusing in the diffraction integral, is not adequate anymore. The true function is given by

$$\exp\left[\mathrm{i}f\frac{1-(1-\mathrm{NA}^2\rho^2)^{1/2}}{1-(1-\mathrm{NA}^2)^{1/2}}\right], \quad 0 \leq \rho \leq 1, \tag{58}$$

in these cases. At the same time, for higher values of NA, one cannot ignore the radiometric effect anymore. Accordingly, the aberration-free pupil function $P \equiv 1$ ($0 \leq \rho \leq 1$) should be changed into

$$(1-\mathrm{NA}^2\rho^2)^{-1/4}, \quad 0 \leq \rho \leq 1. \tag{59}$$

In addition to this, for high values of NA (≥ 0.80), a scalar treatment is not adequate anymore and also the state of polarization should be taken into account, see [30]. For a large part of the medium–high NA regime such as $[0.60, 0.80]$ and when using natural light, it is, however, sufficient to correct according to (58) and (59).

A further complication is caused by the realistic circumstance that one would like to use illumination sources of a non-negligible size so as to have available sufficiently large illumination amplitudes. When the source is a transparent hole of radius a, the pupil function should, in addition, be multiplied by the Fourier transform,

$$J_1(2\pi a\rho)/\pi a\rho, \quad 0 \leq \rho \leq 1, \tag{60}$$

of a normalized disc of radius a.

In this section we present simple measures to take these and similar effects into account, and we present simulation results to show efficacy of these measures.

5.1 *Description of approach*

Taking the effects represented by (58)–(60) into account, the diffraction integral in (4) should be replaced by

$$U(r,\varphi;f\,)=\frac{1}{\pi}\int_0^1\int_0^{2\pi}\exp\left[F(\rho;\mathrm{NA},a)\right]P(\rho,\vartheta)\exp\left[2\pi\mathrm{i}\rho r\cos(\vartheta-\varphi)\right]\rho\,\mathrm{d}\rho\,\mathrm{d}\vartheta,\qquad(61)$$

where $P(\rho,\vartheta)=A(\rho,\vartheta)\exp\left[\mathrm{i}\Phi(\rho,\vartheta)\right]$ is the pupil function and

$$F(\rho;\mathrm{NA},a)=\mathrm{i}f\frac{1-(1-\mathrm{NA}^2\rho^2)^{1/2}}{1-(1-\mathrm{NA}^2)^{1/2}}-\frac{1}{4}\ln(1-\mathrm{NA}^2\rho^2)$$
$$+\ln\left[\frac{J_1(2\pi a\rho)}{\pi a\rho}\right],\quad 0\le\rho\le 1.\qquad(62)$$

For values of NA between 0.6 and 0.8 the function at the right-hand side on the first line of (62) is well approximated by a function of the form $c+\mathrm{d}\rho^2$. Similarly, for values of the radius a in (60) up to the substantial value of 0.4, the function on the second line of (62) admits such an approximation as well. Thus, approximating

$$F(\rho;\mathrm{NA},a)\approx\tilde{g}+\mathrm{i}\tilde{f}\rho^2,\qquad(63)$$

we see that U in (61) is approximated as

$$U(r,\varphi;f\,)\approx\frac{\exp(\tilde{g})}{\pi}\int_0^1\int_0^{2\pi}\exp(\mathrm{i}\tilde{f}\rho^2)P(\rho,\vartheta)\exp\left[2\pi\mathrm{i}\rho r\cos(\vartheta-\varphi)\right]\rho\,\mathrm{d}\rho\,\mathrm{d}\vartheta.\qquad(64)$$

Apart from the factor $\exp(\tilde{g})$, the right-hand side of (64) is exactly of the form (4). This means that the retrieval methods developed in sections 3 and 4 can be applied in the present case as well, just by replacing all $V_n^m(r,f\,)$ by $\exp(\tilde{g})V_n^m(r,f\,)$.

We shall now address the problem of quadratic approximation of a function as we have in (62) for the range $0\le\rho\le 1$. For a smooth function

$$F(\rho)=a_0+a_1\rho^2+a_2\rho^4+\cdots,\quad 0\le\rho\le 1,\qquad(65)$$

the optimal quadratic approximation $\hat{c}+\hat{d}\rho^2$, in the sense that the root mean square error

$$E(F;c,d)=\left(2\int_0^1|F(\rho)-c-d\rho^2|^2\rho\,\mathrm{d}\rho\right)^{1/2}\qquad(66)$$

is minimal for $c=\hat{c}$, $d=\hat{d}$, is given by

$$f_0R_0^0(\rho)+f_2R_2^0(\rho)=(f_0-f_2)+2f_2\rho^2.\qquad(67)$$

Here f_0, f_2 are the first two coefficients in the Zernike[0] expansion $F(\rho)=\sum_{n=0}^{\infty}f_{2n}R_{2n}^0(\rho)$ of F. While these optimal approximations can be obtained in a completely analytic way in many cases (including for the two functions on the first line on the right-hand side of (62), but not for the function on the second line), the developments are rather cumbersome and do not add much insight. Instead, we propose below a device that produces in almost all cases a result of a quality comparable to the optimal result. This device is simple and can be applied in all cases where F is given numerically or analytically. Hence, it equally applies when there are other, application-dependent, effects than those in (58)–(60) that have to be accounted for.

Table 6. RMS error $\hat{E}_n$, $\tilde{E}_n$ for $F(\rho) = \rho^{2n}$.

n	$\hat{E}_n$	$\tilde{E}_n$
0	0	0
1	0	0
2	0.0745	0.0745
3	0.1134	0.1170
4	0.1333	0.1455
5	0.1436	0.1669
10	0.1488	0.2297
100	0.0068	0.3211

We approximate

$$F(\rho) \approx \tilde{c} + \tilde{d}\rho^2, \quad 0 \le \rho \le 1, \tag{68}$$

where

$$\tilde{c} = \tfrac{2}{3}F(0) + \tfrac{2}{3}F(\tfrac{1}{2}2^{1/2}) - \tfrac{1}{3}F(1); \quad \tilde{d} = F(1) - F(0). \tag{69}$$

This approximation results when the fourth degree polynomial $b_0 + b_1\rho^2 + b_2\rho^4$, which coincides with $F(\rho)$, at $\rho = 0, (1/2)2^{1/2}, 1$, and is approximated by a second degree polynomial $c + d\rho^2$ with minimal RMS error value, see (66). It turns out that, when it does make sense to approximate F by a quadratic, the approximation in (68) and (69) is very near to the optimal approximation given above. To demonstrate this, we have included table 6 that shows RMS errors

$$\hat{E}_n := E(\rho^{2n}; \hat{c}, \hat{d}), \quad \tilde{E}_n := E(\rho^{2n}; \tilde{c}, \tilde{d}) \tag{70}$$

for various values of $n = 0, 1, \ldots$. We see from table 6 that rule (68) and (69) yields the optimal choice for $n = 0, 1, 2$, while significant worse performance only occurs for n beyond 5.

We give two examples, relevant in the present context, in which the optimal approximation and the one according to (68) and (69) are compared. We have

$$\begin{aligned} 1 - \left[1 - (0.8)^2\rho^2\right]^{1/2} &\approx -0.014166 + 0.395\rho^2 \\ &\approx -0.016414 + 0.4\rho^2, \end{aligned} \tag{71}$$

where the first line gives the optimal approximation, with RMS error 0.00731, and the second line gives the approximation in (68) and (69), with RMS error 0.00746. Also we have with $a = 1/\pi$ in (60)

$$\begin{aligned} \ln\left[\frac{J_1(2\rho)}{\rho}\right] &\approx 0.008684 - 0.549298\rho^2 \\ &\approx 0.009209 - 0.550390\rho^2, \end{aligned} \tag{72}$$

where the first line gives the optimal approximation, with RMS error 0.004116, and the second line gives the approximation in (68) and (69), with RMS error 0.004129.

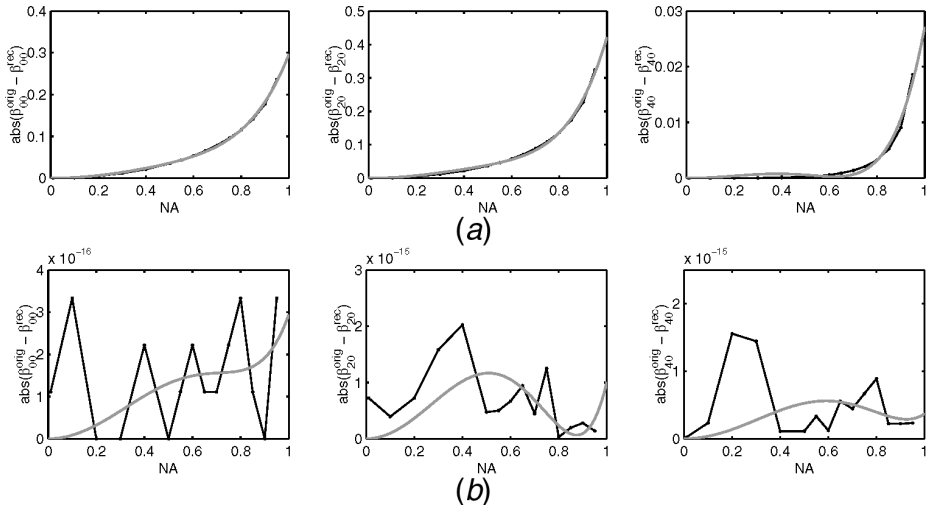

Figure 13. Reconstruction errors for an aberration-free pupil using (*a*) the uncorrected $V_n^m(r,f)$ and (*b*) the corrected $\exp[\tilde{g}]V_n^m(r,\tilde{f})$ for various values of NA.

5.2 *Simulations*

(a) We consider an aberration-free pupil function $P \equiv 1$, so that $\beta_n^m = \delta_{m0}\delta_{n0}$, and we assume a non-zero value for NA and $a = 0$ in the diffraction integral (61). We have not been able to find a (simple) analytic computation scheme for the resulting U in (61) (an analytic but complicated scheme has been presented in [61], Appendix B). Therefore, we have chosen to approximate the U of (61) by the right-hand side of (64) with $\tilde{f}, \tilde{g}$ given by the device developed in (68) and (69). In figure 13(*a*) and (*b*) we show the reconstruction errors for β_0^0, β_2^0, β_4^0, where the measured intensity $|U|^2$ ($\approx$ | right-hand side of (64)|^2) is being matched using the original, uncorrected $V_n^m(r,f)$ (figure 13(*a*)) and the corrected $\exp[\tilde{g}]V_n^m(r,\tilde{f})$ (figure 13(*b*)) respectively. We may concentrate on the systems in (51) ($m = 0$) and we use $n, n' = 0, 2, 4$. We thus see that serious errors occur in the uncorrected case while errors on the level of machine precision occur (as is to be expected) in the corrected case. The solid lines in figure 13(*a*) and (*b*) indicate best fit $c_1\mathrm{NA}^2 + c_2\mathrm{NA}^4 + c_3\mathrm{NA}^6$ to the reconstruction errors at NA $= 0$ to NA $= 0.9$.

(b) We next consider an aberration-free pupil function $P \equiv 1$, where we now assume NA $= 0$ and $a = b/2\pi > 0$ in the diffraction integral in (61). Accordingly, U is now given by

$$U(r, \vartheta; f) = \int_0^1 \frac{2J_1(b\rho)}{b\rho} \exp(\mathrm{i}f\rho^2) J_0(2\pi\rho r)\rho \, \mathrm{d}\rho \tag{73}$$

and the measured intensity can be computed as $|2\sum_p C_p(b)V_{2p}^0|$ where the Zernike coefficients $C_p(b)$ in the appendix, (A 26) and (A 27), of $2J_1(b\rho)/b\rho$ are used and $p = 0, 1, 2$. In figure 14(*a*) and (*b*), we show the reconstruction errors for $\beta_0^0, \beta_2^0, \beta_4^0$ where the measured intensity is being matched using the

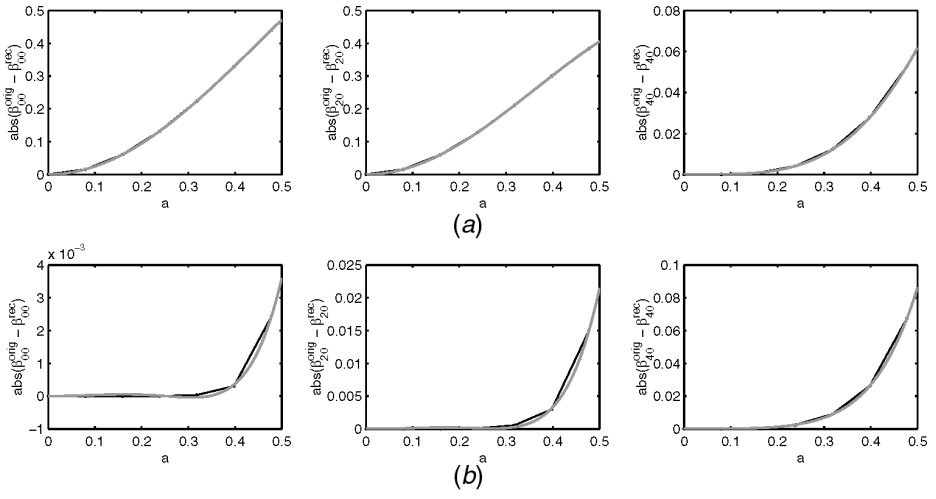

Figure 14. Reconstruction errors for an aberration-free pupil using (*a*) the uncorrected $V_n^m(r,f)$ and (*b*) the corrected $\exp[\tilde{g}]V_n^m(r,\tilde{f})$ for various hole sizes $a = b/2\pi$.

original, uncorrected $V_n^m(r,f)$ (figure 14(*a*)) and the corrected $\exp[\tilde{g}]V_n^m(r,\tilde{f})$ (figure 14(*b*)), respectively. The correction quantities $\tilde{f},\tilde{g}$ were computed using the device developed in (68) and (69). We thus see that the serious reconstruction errors in the uncorrected case are almost eliminated for a as large as 0.4 by correcting the V_n^m functions. This is especially so for β_0^0, β_2^0, but not for β_4^0 (which is to be expected).

(c) We repeat the previous exercise with a comatic pupil function $P(\rho,\vartheta) = \exp[\mathrm{i}\alpha Z_3^1(\rho,\vartheta)]$, $\alpha = 0.1$. The measured intensity can be computed as $|2\sum_{n,m}\beta_n^m V_n^m(r,f)\cos m\vartheta|^2$ with β_n^m given in the appendix, (A 19) and (A 20), where the summation extends over all relevant m,n with $m \le 4, n \le 9$. We aim at retrieving the quantities ${}_3^1\beta_n^m(\alpha)$ of the appendix, (A 18), these being the Zernike coefficients of the pupil function P. In figure 15(*a*) and (*b*) we show the reconstruction errors for $\beta_0^0, \beta_3^1, \beta_4^0, \beta_6^2$ without and with corrections being made on the V_n^m functions. The retrieval is hence performed for $m = 0,1,2$ and $n = n' = [0,2,4,6,8]$, $[1,3,5,7,9]$, $[2,4,6,8]$ respectively. Furthermore, in figure 16 we see what happens when the predictor–corrector approach is used.

From figure 15(*a*) we see that the error in the amount of coma being retrieved is increasing with hole size a. In figure 15(*b*) we see that when using the corrected V_n^m functions, the amount of coma is retrieved accurately up to a hole size $a = 0.4$ and then increases. However, the result for $a = 0.4$ is still satisfactory. Moreover, the application of the correction on the V_n^m functions delivers very accurate estimates of the DC term of the transmission, as can be seen in the top graph of figure 15(*b*). In figure 16(*a*) and (*b*) we see again the effect that the initial guesses are all better when using the corrected V_n^m functions. Moreover, we see that the reconstruction errors after a few iterations settle at much smaller values.

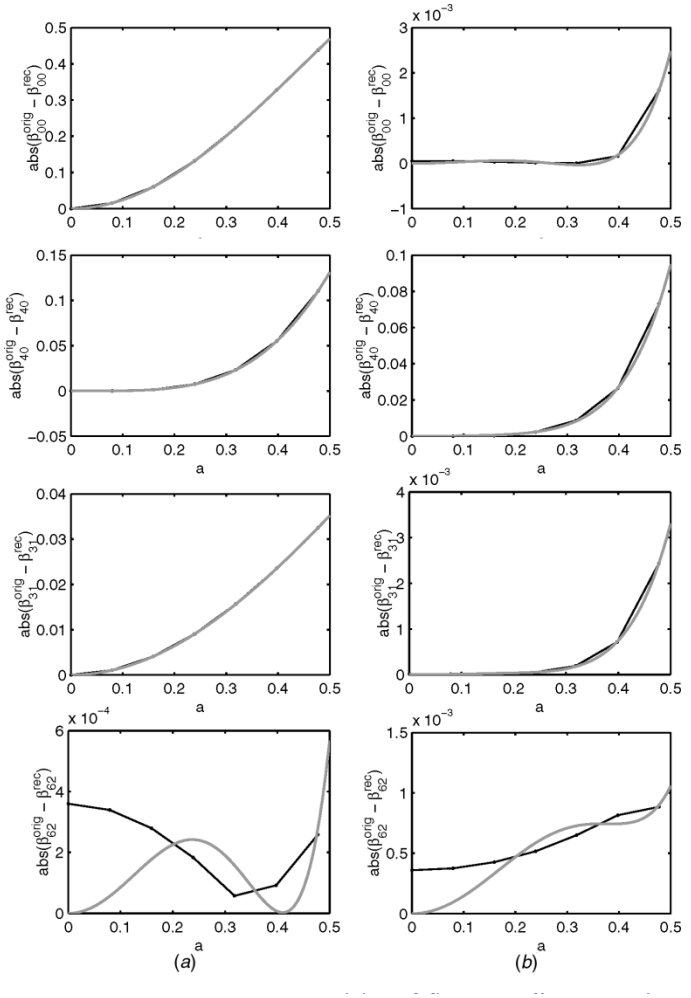

Figure 15. Reconstruction errors of four different coefficients as a function of hole size a. Coma $\alpha = 0.1$. Reconstruction using (a) uncorrected and (b) corrected V_n^m functions. Note the different scales on the vertical axes.

6. Conclusions and outlook

We have presented and analysed a method for the retrieval of pure-phase aberrations and its extension to the case of retrieval of general aberrations from the observation of the intensity point-spread function in the focal region. In these methods, the complex amplitude of the point-spread function is represented in terms of the Zernike coefficients describing the aberrated pupil function, and these coefficients are estimated by matching the observed intensity and the (linearized) theoretical intensity in the focal region. We have discussed particular features of either method, such as occurrence of third-order error behaviour in the pure-phase retrieval method

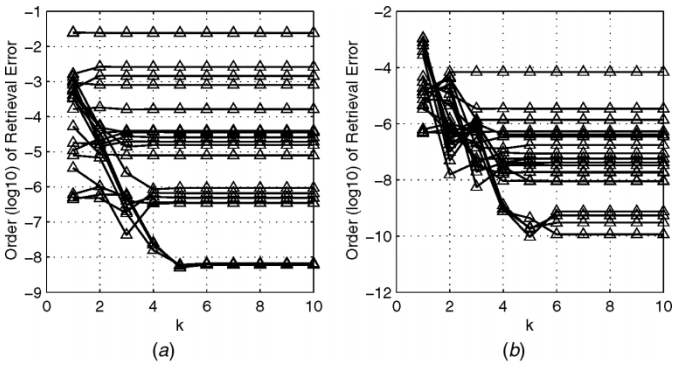

Figure 16. The effect on the predictor–corrector approach. Hole size $a = 0.1$, coma $\alpha = 0.1$. Iteration histories (k) using (a) uncorrected and (b) corrected V_n^m functions.

and the potential of perfect reconstruction by adopting a predictor–corrector approach for the general retrieval method, and we have briefly indicated their application range by presenting results of simulations. While the pure-phase method gives good results for aberrations up to somewhat below the diffraction limit, the general method (in its predictor–corrector version) seems to be capable of retrieving aberrations well beyond this limit. The methods have been extended in a simple and straightforward way to the case of medium–high numerical apertures and to the case that the illumination source has a lateral size somewhat larger than the diffraction unit.

There are many more things that could have been simulated, but we have restricted ourselves here to those simulations that highlight characteristic features of the methods. We now list a number of issues that should be addressed when the methods are considered in more detail with respect to their usefulness in practice. This list includes

(a) investigation of the required sizes of the linear systems from which the estimates are extracted,
(b) a more extensive investigation of the effects of the various discretization and finitization operations,
(c) a more extensive investigation of the influence of various types of noise,
(d) influence of instrument function for data acquisition,
(e) the effects of mismodelling, such as incorrectly specified pupil radius and numerical aperture, as well as misalignment of the focal planes,
(f) measures to be taken when data acquisition is only possible on a discrete set of curves,
(g) sensitivity of the methods for DC offsets in the recorded intensities,
(h) consideration of optical systems with a central obstruction,
(i) use of the predictor–corrector method with relaxation,
(j) the impact of the method in section 5 to account for the effects discussed there on the level of Zernike coefficients.

There are also some fundamental aspects of the methods that should be addressed. These include an investigation of the problem of (approximately) representing an intensity I_{meas} as $|\sum_{n,m}\beta_n^m U_n^m|^2$, with issues such as existence and uniqueness of the β's as well as the choice of appropriate error functionals. Furthermore, a statistical analysis is needed for the methods aimed at quality assessment of the estimates obtained from noisy data (Cramer–Rao bounds, etc.). Such an assessment is also required for the estimates obtained by the methods when the predictor–corrector option is switched off since these estimates carry an intrinsic error due to linearizations. Also, further analysis, experiments and simulations are required to get a better insight into the convergence behaviour of the predictor–corrector approach, especially when the optical system is heavily aberrated. In this connection, it would be interesting to further investigate the β's and their saturation levels in the cases that the intensities I_{meas} cannot be perfectly represented as $|\sum_{n,m}\beta_n^m U_n^m|^2$ due to noise and/or modelling errors as we had in sections 4 and 5. The results presented in this paper, as well as experimental results obtained in a lithographic context, are promising enough so that further investigation of the method with respect to these and other aspects is justified.

Appendix: Some Zernike expansions

In this appendix we present the Zernike expansions in analytic form of the pupil functions

$$\exp[\mathrm{i}\alpha R_4^0(\rho)], \quad \exp[\mathrm{i}\alpha R_3^1(\rho)\cos\vartheta], \quad \frac{2J_1(b\rho)}{b\rho}, \tag{A 1}$$

that are required for the simulations in sections 3, 4 and 5.

When $P(\rho,\vartheta)$ is a (symmetric) pupil function, its Zernike expansion coefficients β_n^m in

$$P(\rho,\vartheta)=\sum_{n,m}\beta_n^m R_n^m(\rho)\cos m\vartheta \tag{A 2}$$

are given from orthogonality of the Zernike functions, see [23], formula (3) on p. 523, as

$$\beta_n^m=\frac{1}{\pi}(n+1)\varepsilon_m\int_0^1\int_0^{2\pi}P(\rho,\vartheta)R_n^m(\rho)\cos m\vartheta\rho\,\mathrm{d}\rho\,\mathrm{d}\vartheta \tag{A 3}$$

with ε Neumann's symbol, $\varepsilon_0=1$, $\varepsilon_1=\varepsilon_2=\cdots=2$.

In the case of $\exp[\mathrm{i}\alpha R_4^0(\rho)]$, all β_n^m with $m\neq 0$ vanish, and for $m=0$, $n=2p$ we have

$$\beta_n^m=2(2p+1)\int_0^1\exp[\mathrm{i}\alpha R_4^0(\rho)]R_{2p}^0(\rho)\rho\,\mathrm{d}\rho=:{}_4\beta_{2p}^0(\alpha). \tag{A 4}$$

With

$$R_4^0(\rho)=6\rho^4-6\rho^2+1=\tfrac{3}{2}(2\rho^2-1)^2-\tfrac{1}{2}, \quad R_{2p}^0(\rho)=P_p(2\rho^2-1), \tag{A 5}$$

where P_p is the pth Legendre polynomial, we get by the substitution $x = 2\rho^2 - 1$ that

$$ {}^{0}_{4}\beta^{0}_{2p}(\alpha) = \left(p + \frac{1}{2}\right) \exp\left(-\frac{1}{2}\mathrm{i}\alpha\right) \int_{-1}^{1} \exp\left(\frac{3}{2}\mathrm{i}\alpha x^2\right) P_p(x)\,\mathrm{d}x. \tag{A 6} $$

Since $P_p(x)$ is odd in x when p is odd and even in x when p is even, we only have to consider the case that $p = 2r$ in (A 6). By power series expansion of $\exp((3/2)\mathrm{i}\alpha x^2)$ we obtain for $p = 2r$

$$ {}^{0}_{4}\beta^{0}_{4r}(\alpha) = \left(p + \frac{1}{2}\right) \exp\left(-\frac{1}{2}\mathrm{i}\alpha\right) \sum_{k=0}^{\infty} \frac{((3/2)\mathrm{i}\alpha)^k}{k!} \int_{-1}^{1} x^{2k} P_{2r}(x)\,\mathrm{d}x. \tag{A 7} $$

The remaining integrals in (A 7) can be evaluated by using Rodriguez' formula, see [31], formula (10.4) on p. 190,

$$ P_p(x) = \frac{(-1)^p}{2^p p!} \left(\frac{\mathrm{d}}{\mathrm{d}x}\right)^p (1 - x^2)^p, p = 0, 1, \ldots. \tag{A 8} $$

Thus, by $2r$ partial integrations, we get

$$ \int_{-1}^{1} x^{2k} P_{2r}(x)\,\mathrm{d}x = \frac{(2k)!}{2^{2r}(2r)!(2k - 2r)!} \int_{-1}^{1} (1 - x^2)^{2r} x^{2k-2r}\,\mathrm{d}x, \quad k \geq r, \tag{A 9} $$

while the integral on the left-hand side vanishes for $k < r$. The remaining integral can be expressed in terms of the beta-function [32], and we find after some manipulations

$$ \int_{-1}^{1} x^{2k} P_{2r}(x)\,\mathrm{d}x = 4^{r+1} \frac{(2k)!(k + r + 1)!}{(2k + 2r + 2)!(k - r)!}, \quad k \geq r. \tag{A 10} $$

Using this in (A 7) and shifting the summation index by r, we obtain

$$ {}^{0}_{4}\beta^{0}_{4r}(\alpha) = 4\left(2r + \frac{1}{2}\right) \exp\left(-\frac{1}{2}\mathrm{i}\alpha\right) \sum_{k=0}^{\infty} \frac{((3/2)\mathrm{i}\alpha)^k}{k!} \frac{(2k + 2r)!(k + 2r + 1)!}{(2k + 4r + 2)!(k + r)!}. \tag{A 11} $$

Finally, this can be brought into a hypergeometric form,

$$ {}^{0}_{4}\beta^{0}_{4r}(\alpha) = \exp\left(-\frac{1}{2}\mathrm{i}\alpha\right) \frac{((3/2)\mathrm{i}\alpha)^r}{(r + (1/2))_r} \sum_{k=0}^{\infty} \frac{((3/2)\mathrm{i}\alpha)^k}{k!} \frac{(r + (1/2))_k}{(2r + (3/2))_k}, \tag{A 12} $$

after some further manipulations using Pochhammer's symbol

$$ (a)_0 = 1; \quad (a)_k = a(a + 1)\cdots(a + k - 1), \quad k = 1, 2, \ldots. \tag{A 13} $$

We shall next compute the Zernike expansion coefficients ${}^{1}_{3}\beta^{m}_{n}(\alpha)$ of $P(\rho, \vartheta) = \exp[\mathrm{i}\alpha R^1_3(\rho)\cos\vartheta]$. The integral in (A 3) over ϑ can be done using (7) and we obtain

$$ {}^{1}_{3}\beta^{m}_{n}(\alpha) = 2(n + 1)\varepsilon_m \mathrm{i}^m \int_0^1 R^m_n(\rho) J_m(\alpha R^1_3(\rho))\rho\,\mathrm{d}\rho. \tag{A 14} $$

Inserting the series expansion of J_m, see [32], formula 9.1.10 on p. 360, into the right-hand side integral in (A 14), we find

$$ {}_3^1\beta_n^m(\alpha) = 2(n+1)\varepsilon_m \mathrm{i}^m \sum_{j=0}^{\infty} \frac{(-1)^j((1/2)\alpha)^{m+2j}}{j!(j+m)!} \int_0^1 (R_3^1(\rho))^{m+2j} R_n^m(\rho)\rho \,\mathrm{d}\rho. \tag{A 15} $$

The remaining integrals can be evaluated by using that $R_3^1(\rho) = 3\rho^3 - 2\rho$, Newton's binomium, and the fact that, see [29], formula (A 2) on p. 2289,

$$ \int_0^1 \rho^{m+2s} R_{m+2p}^m(\rho)\rho \,\mathrm{d}\rho = \frac{1}{2}(-1)^p \frac{(-s)_p}{(m+s+1)_{p+1}}, \tag{A 16} $$

where we have used Pochhammer's symbol (A 13). This yields

$$ \int_0^1 (R_3^1(\rho))^{m+2j} R_{m+2p}^m(\rho)\rho \,\mathrm{d}\rho = \frac{1}{2}(-2)^{m+2j} \sum_{l=0}^{m+2j} \binom{m+2j}{l} \left(\frac{-3}{2}\right)^l \frac{(-j-l)_p(-1)^p}{(m+j+l+1)_{p+1}}, \tag{A 17} $$

and with some final rewriting we obtain

$$ \begin{aligned} {}_3^1\beta_{m+2p}^m(\alpha) = (m+2p+1)\varepsilon_m &\sum_{j=0}^{\infty} \frac{(-\mathrm{i}\alpha)^{m+2j}}{j!(j+m)!} \\ &\times \sum_{l=0}^{m+2j} \binom{m+2j}{l} \frac{(-1)^p(-j-l)_p}{(m+j+l+1)_{p+1}} \left(-\frac{3}{2}\right)^l. \end{aligned} \tag{A 18} $$

In a similar fashion we can determine the Zernike expansion coefficients β_n^m of $P(\rho,\vartheta) = A(\rho)\exp[\mathrm{i}\alpha R_3^1(\rho)\cos\vartheta]$, where $A(\rho)$ is an amplitude function admitting the power series representation $A(\rho) = \sum_{k=0}^{\infty} a_k \rho^{2k}$. Inserting this power series into the above derivation, it can be shown that

$$ \begin{aligned} \beta_{m+2p}^m = (m+2p+1)\varepsilon_m &\sum_{k=0}^{\infty} a_k \sum_{j=0}^{\infty} \frac{(-\mathrm{i}\alpha)^{m+2j}}{j!(j+m)!} \\ &\times \sum_{l=0}^{m+2j} \binom{m+2j}{l} \frac{(-1)^p(-j-l-k)_p}{(m+j+l+k+1)_{p+1}} \left(-\frac{3}{2}\right)^l. \end{aligned} \tag{A 19} $$

In section 5.2, point (c), we use this with

$$ \frac{2J_1(b\rho)}{b\rho} = \sum_{k=0}^{\infty} a_k \rho^{2k}; \quad a_k = \frac{(-1)^k((1/2)b)^{2k}}{k!(k+1)!}. \tag{A 20} $$

We finally determine the Zernike expansion of $2J_1(b\rho)/b\rho$. We have that β_n^m vanishes for all $m \neq 0$ and for $m = 0$, $n = 2p$ we have

$$ \beta_n^m = 4(2p+1) \int_0^1 \frac{J_1(b\rho)}{b\rho} R_{2p}^0(\rho)\rho \,\mathrm{d}\rho =: C_p(b). \tag{A 21} $$

Using [32], first identity in 9.1.30 on p. 361, so that

$$ \frac{J_1(b\rho)}{b\rho} = \int_0^1 J_0(b\rho\rho_1)\rho_1 \,\mathrm{d}\rho_1, \tag{A 22} $$

we get by changing the order of integration

$$C_p(b) = 4(2p+1)\int_0^1 \left(\int_0^1 J_0(b\rho\rho_1) R_{2p}^0(\rho)\rho \,\mathrm{d}\rho \right) \rho_1 \,\mathrm{d}\rho_1. \tag{A 23}$$

Using for the inner integral the basic result

$$\int_0^1 R_n^m(\rho) J_m(\rho r)\rho \,\mathrm{d}\rho = (-1)^{(n-m)/2} \frac{J_{n+1}(r)}{r} \tag{A 24}$$

from the 'classical' Nijboer–Zernike theory, see [23], formula (9) on p. 525, we get

$$C_p(b) = 4(2p+1)b^{-2} \int_0^b J_{2p+1}(t) \,\mathrm{d}t. \tag{A 25}$$

Finally, we use [32], formula 11.1.4 on p. 480, and we find

$$C_p(b) = 4(2p+1)\frac{(-1)^p}{b^2} \left\{ 1 - J_0(b) - 2\sum_{l=1}^{p} J_{2l}(b) \right\}. \tag{A 26}$$

Alternatively, from [32], formula 9.1.10 on p. 360 we readily obtain

$$C_p(b) = (2p+1)\sum_{k=0}^{\infty} \frac{(-(1/4)b^2)^{k+p}}{k!(k+2p+1)!(k+p+1)}. \tag{A 27}$$

References

[1] T.A. Brunner, IBM J. Res. Dev. **41** 57 (1997).
[2] D.G. Flagello, H. van der Laan, J. van Schoot, *et al*., Proc. SPIE **3679** 162 (1999).
[3] N.R. Farrar, A.L. Smith, D. Busath, *et al*., Proc. SPIE **4000** 18 (2000).
[4] J.P. Kirk and T.A. Brunner, Proc. SPIE **2726** 410 (1996).
[5] P. Dirksen, C. Juffermans, R. Pellens, *et al*., Proc. SPIE **3679** 77 (1999).
[6] F. Zach, C.Y. Lin and J.P. Kirk, Proc. SPIE **4346** 1362 (2001).
[7] P. Dirksen, J.J.M. Braat, A.J.E.M. Janssen, *et al*., J. Microlith. Microfab. Microsyst. **2** 61 (2003).
[8] R.W. Gerchberg and W.O. Saxton, Optik. **34** 275 (1971).
[9] R.W. Gerchberg and W.O. Saxton, Optik. **35** 237 (1972).
[10] B.R. Frieden, J. Opt. Soc. Am. **62** 511 (1972).
[11] W.H. Richards, J. Opt. Soc. Am. **62** 55 (1972).
[12] J.R. Fienup, Appl. Opt. **21** 2758 (1982).
[13] J.R. Fienup, J.C. Marron, T.J. Schultz, *et al*., Appl. Opt. **32** 1747 (1993).
[14] J.G. Walker, Opt. Acta **28** 735 (1981).
[15] R. Gonsalves, Opt. Eng. **21** 829 (1982).
[16] J.R. Fienup, J. Opt. Soc. Am. A **16** 1831 (1999).
[17] D. van Dyck and W. Coene, Optik. **77** 125 (1987).
[18] B.R. Frieden and C. Oh, Appl. Opt. **31** 1103 (1992).
[19] E.S. Angel and A.K. Jain, Appl. Opt. **17** 2186 (1978).
[20] R. Barakat and B.H. Sandler, J. Opt. Soc. Am. A **19** 1715 (1992).
[21] I. Iglesias, Appl. Opt. **37** 5427 (1998).
[22] A.J.E.M. Janssen, J. Opt. Soc. Am. A **19** 849 (2002).
[23] M. Born and E. Wolf, *Principles of Optics* (Cambridge University Press, Cambridge, 2002).
[24] A.J.E.M. Janssen, J.J.M. Braat and P. Dirksen, J. Mod. Opt. **51** 687 (2004).
[25] J.J.M. Braat, P. Dirksen and A.J.E.M. Janssen, J. Opt. Soc. Am. A **19** 858 (2002).

[26] P. Dirksen, J.J.M. Braat, P. De Bisschop, *et al*., Proc. SPIE **4691** 1392 (2002).
[27] P. Dirksen, J. Braat, A.J.E.M. Janssen, *et al*., Proc. SPIE **5040** 1 (2003).
[28] P. Dirksen, J.J.M. Braat, A.J.E.M. Janssen, *et al*., Proc. SPIE **5377** 150 (2004).
[29] J.J.M. Braat, P. Dirksen, A.J.E.M. Janssen, *et al*., J. Opt. Soc. Am. A **20** 2281 (2003).
[30] J.J.M. Braat, P. Dirksen and A.J.E.M. Janssen, submitted to JOSA - A (2004).
[31] F.G. Tricomi, *Vorlesungen über Orthogonalreihen* (Springer, Berlin, 1955).
[32] M. Abramowitz and I.A. Stegun, *Handbook of Mathematical Functions* (Dover, New York, 1970).